Non-linear beam dynamics

Yannis PAPAPHILIPPOU
Accelerator and Beam Physics group
Beams Department
CERN

Università di Roma, La Sapienza

Rome, ITALY

20-23 June 2016

Contents of the 4th lecture

- Chaos detection methods and frequency map analysis
  - Dynamic aperture
  - Quasi-periodic motion
  - The NAFF algorithm
  - Frequency determination and precision
  - Aspects of frequency maps
- Simulation studies
  - Frequency and diffusion maps for the LHC
  - Beam-beam effect
  - Folded frequency maps
  - Magnet fringe-fields
  - Working point choice
  - Resonance free lattice
  - Symplectic integration
  - Correction schemes evaluation
- Experiments
  - Experimental frequency maps
  - Beam loss frequency maps
  - Space-charge frequency scan
- Summary

Contents of the 4th lecture

- Chaos detection methods and frequency map analysis
  - Dynamic aperture
  - Quasi-periodic motion
  - The NAFF algorithm
  - Frequency determination and precision
  - Aspects of frequency maps
- Simulation studies
  - Frequency and diffusion maps for the LHC
  - Beam-beam effect
  - Folded frequency maps
  - Magnet fringe-fields
  - Working point choice
  - Resonance free lattice
  - Symplectic integration
  - Correction schemes evaluation
- Experiments
  - Experimental frequency maps
  - Beam loss frequency maps
  - Space-charge frequency scan
- Summary

Chaos detection methods

- Computing/measuring dynamic aperture (DA) or particle survival

  A. Chao et al., PRL 61, 24, 2752, 1988;
  F. Willeke, PAC95, 24, 109, 1989.

- Computation of Lyapunov exponents

  F. Schmidt, F. Willeke and F. Zimmermann, PA, 35, 249, 1991;
  M. Giovannozi, W. Scandale and E. Todesco, PA 56, 195, 1997

- Variance of unperturbed action (a la Chirikov)

  B. Chirikov, J. Ford and F. Vivaldi, AIP CP-57, 323, 1979
  J. Tennyson, SSC-155, 1988;
  J. Irwin, SSC-233, 1989

- Fokker-Planck diffusion coefficient in actions

  T. Sen and J.A. Elisson, PRL 77, 1051, 1996

- **Frequency map analysis**

Dynamic Aperture

- The most direct way to evaluate the non-linear dynamics performance of a ring is the computation of **Dynamic Aperture**
- Particle motion due to multi-pole errors is generally non-bounded, so chaotic particles can **escape to infinity**
- This is not true for all non-linearities (e.g. the beam-beam force)
- Need a **symplectic** tracking code to follow particle trajectories (a lot of initial conditions) for a **number of turns** (depending on the given problem) until the particles start getting lost. This **boundary** defines the **Dynamic aperture**
- As multi-pole errors may not be completely known, one has to track through **several machine models** built by **random distribution** of these errors
- One could start with 4D (only transverse) tracking but certainly needs to simulate 5D (constant energy deviation) and finally 6D (synchrotron motion included)

Dynamic Aperture plots

- Dynamic aperture plots show the maximum initial values of stable trajectories in x-y coordinate space at a particular point in the lattice, for a range of energy errors.
  - The beam size can be shown on the same plot.
  - Generally, the goal is to allow some significant margin in the design - the measured dynamic aperture is often smaller than the predicted dynamic aperture.

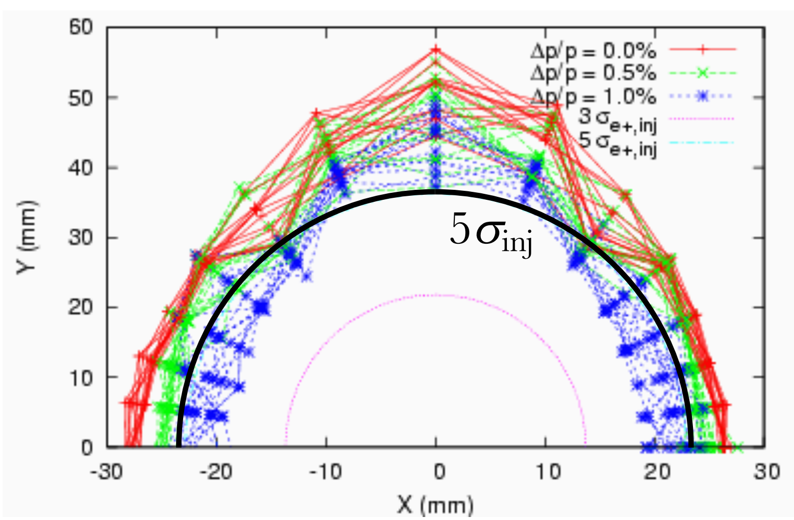

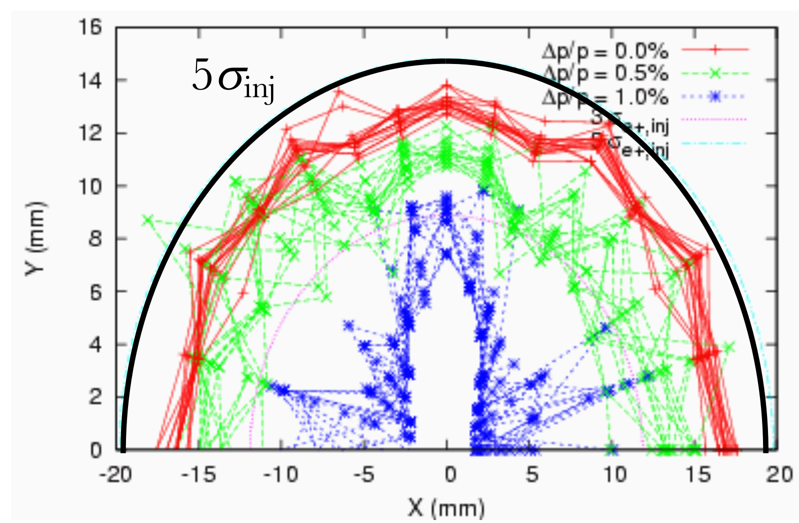

Dynamic aperture including damping

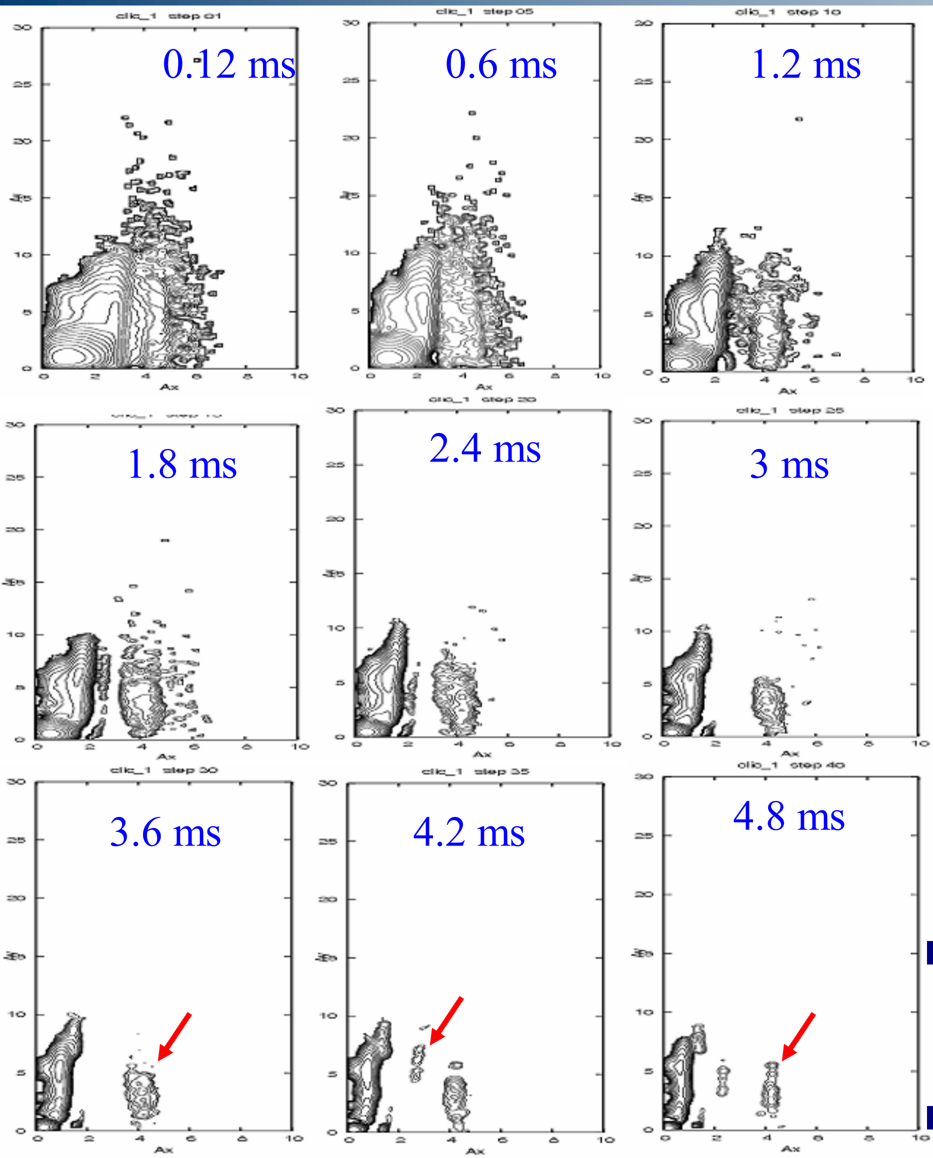

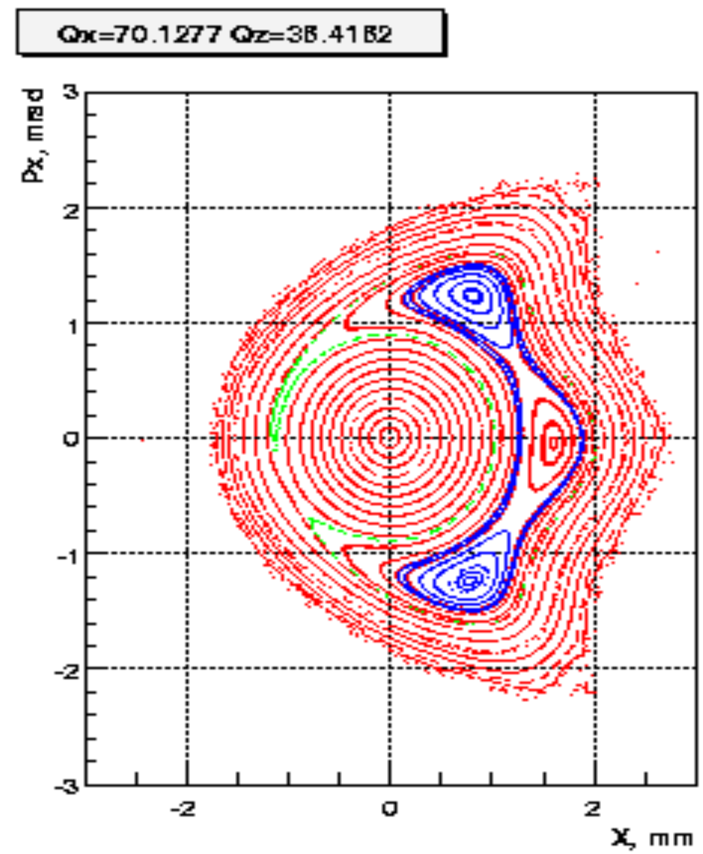

- Including radiation damping and excitation shows that 0.7% of the particles are lost during the damping
- Certain particles seem to damp away from the beam core, on resonance islands

Genetic Algorithms for lattice optimisation

- MOGA –Multi Objective Genetic Algorithms are being recently used to optimise linear but also non-linear dynamics of electron low emittance storage rings
- Use knobs quadrupole strengths, chromaticity sextupoles and correctors with some constraints
- Target ultra-low horizontal emittance, increased lifetime and high dynamic aperture

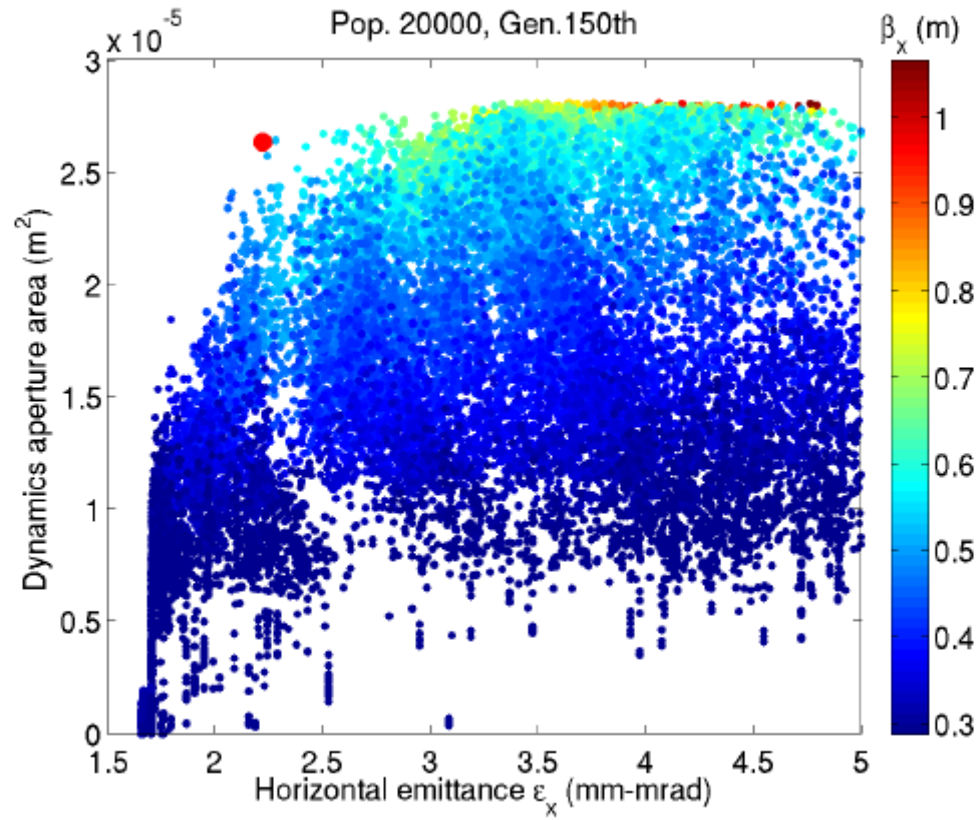

Measuring Dynamic Aperture

- During LHC design phase, DA target was 2x higher than collimator position, due to statistical fluctuation, finite mesh, linear imperfections, short tracking time, multi-pole time dependence, ripple and a 20% safety margin
- Better knowledge of the model led to good agreement between measurements and simulations for actual LHC
- Necessity to build an accurate magnetic model (from beam based measurements)

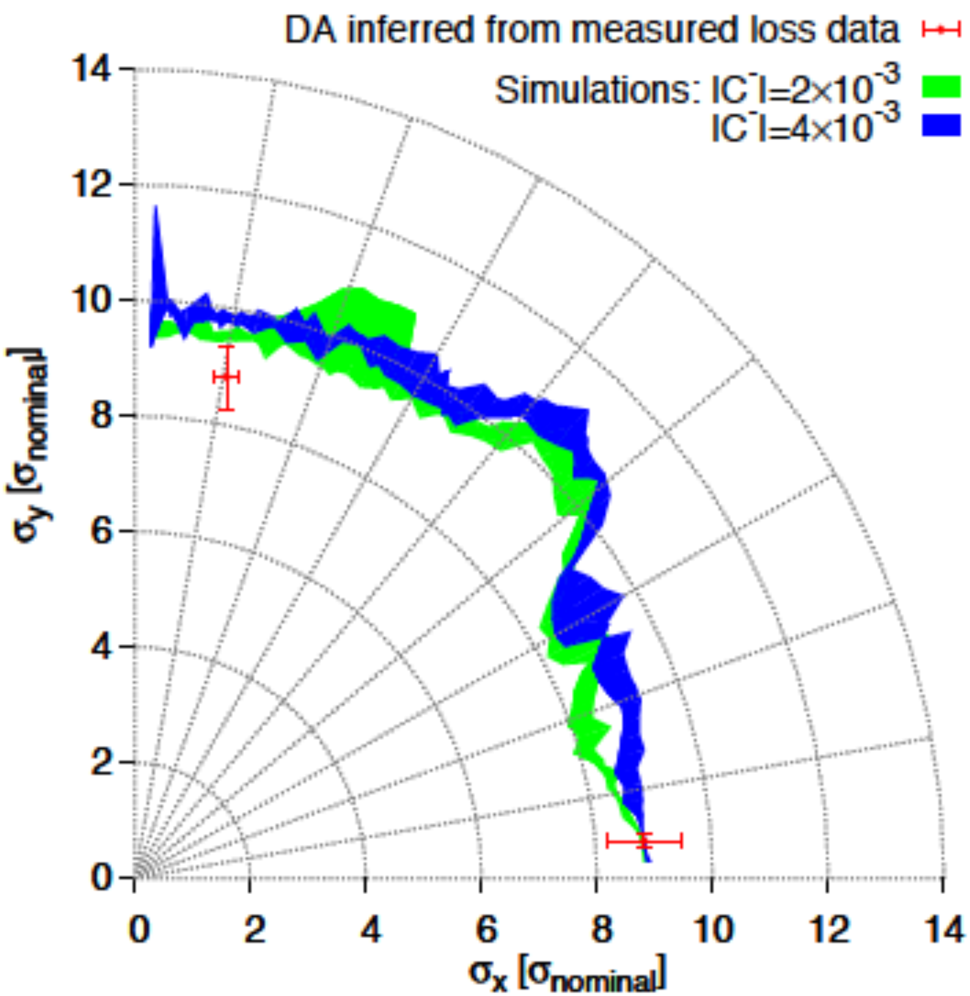

Frequency map analysis

- Frequency Map Analysis (FMA) is a numerical method which springs from the studies of J. Laskar (Paris Observatory) putting in evidence the chaotic motion in the Solar Systems
- FMA was successively applied to several dynamical systems
  - Stability of Earth Obliquity and climate stabilization (Laskar, Robutel, 1993)
  - 4D maps (Laskar 1993)
  - Galactic Dynamics (Y.P and Laskar, 1996 and 1998)
  - Accelerator beam dynamics: lepton and hadron rings (Dumas, Laskar, 1993, Laskar, Robin, 1996, Y.P, 1999, Nadolski and Laskar 2001)

Motion on torus

- Consider an integrable Hamiltonian system of the usual form

$$H(\boldsymbol{J}, \boldsymbol{\varphi}, \theta) = H_0(\mathbf{J})$$

- Hamilton's equations give

$$\dot{\phi}_j = \frac{\partial H_0(\mathbf{J})}{\partial J_j} = \omega_j(\mathbf{J}) \Rightarrow \phi_j = \omega_j(\mathbf{J})t + \phi_{j0}$$

$$\dot{J}_j = -\frac{\partial H_0(\mathbf{J})}{\partial \phi_j} = 0 \Rightarrow J_j = \text{const.}$$

- The actions define the surface of an invariant torus
- In complex coordinates the motion is described by

$$\zeta_j(t) = J_j(0)e^{i\omega_j t} = z_{j0}e^{i\omega_j t}$$

- For a **non-degenerate** system $\det\left|\frac{\partial\omega(J)}{\partial J}\right| = \det\left|\frac{\partial^2 H_0(J)}{\partial J^2}\right| \neq 0$ there is a one-to-one correspondence between the actions and the frequency, a frequency map can be defined parameterizing the tori in the frequency space

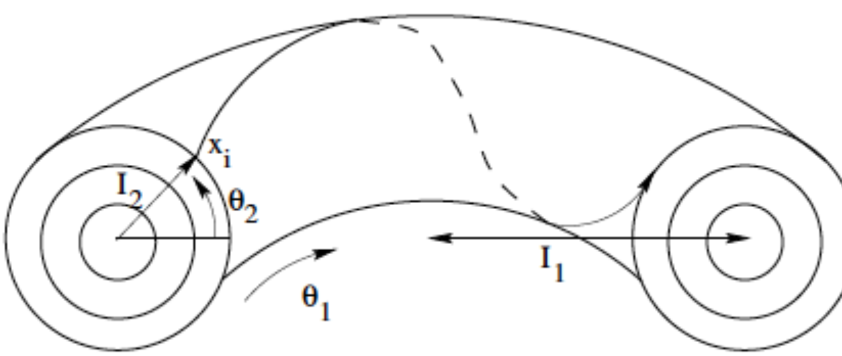

$$F: \quad (\mathbf{I}) \longrightarrow (\omega)$$

Quasi-periodic motion

- If a transformation is made to some new variables

$$\zeta_j = I_j e^{i\theta_j t} = z_j + \epsilon G_j(\mathbf{z}) = z_j + \epsilon \sum_{\mathbf{m}} c_{\mathbf{m}} z_1^{m_1} z_2^{m_2} \ldots z_n^{m_n}$$

- The system is still integrable but the tori are distorted
- The motion is then described by

$$\zeta_j(t) = z_{j0} e^{i\omega_j t} + \sum_{\mathbf{m}} a_{\mathbf{m}} e^{i\,(\mathbf{m}\cdot\omega)\,t}$$

i.e. a quasi-periodic function of time, with

$$a_{\mathbf{m}} = \epsilon\, c_{\mathbf{m}} z_{10}^{m_1} z_{20}^{m_2} \ldots z_{n0}^{m_n} \text{ and } \mathbf{m}\cdot\omega = m_1\omega_1 + m_2\omega_2 + \cdots + m_n\omega_n$$

- For a non-integrable Hamiltonian, $H(\mathbf{I},\theta) = H_0(\mathbf{I}) + \epsilon H'(\mathbf{I},\theta)$ and especially if the perturbation is small, most tori persist (**KAM** theory)
- In that case, the motion is still quasi-periodic and a frequency map can be built
- The regularity (or not) of the map reveals stable (or chaotic) motion

Building the frequency map

- When a quasi-periodic function $f(t) = q(t) + ip(t)$ in the complex domain is given numerically, it is possible to recover a quasi-periodic approximation

$$f'(t) = \sum_{k=1}^{N} a'_k e^{i\omega'_k t}$$

in a very precise way over a finite time span $[-T, T]$ several orders of magnitude more precisely than simple Fourier techniques

- This approximation is provided by the Numerical Analysis of Fundamental Frequencies – **NAFF** algorithm
- The frequencies ω'_k and complex amplitudes a'_k are computed through an iterative scheme.

The NAFF algorithm

- The first frequency ω_1' is found by the location of the maximum of

$$\phi(\sigma) = \langle f(t), e^{i\sigma t} \rangle = \frac{1}{2T}\int_{-T}^{T} f(t)e^{-i\sigma t}\chi(t)dt$$

  where $\chi(t)$ is a weight function
- In most of the cases the Hanning window filter is used $\chi_1(t) = 1 + \cos(\pi t/T)$
- Once the first term $e^{i\omega_1' t}$ is found, its complex amplitude a_1' is obtained and the process is restarted on the remaining part of the function

$$f_1(t) = f(t) - a_1' e^{i\omega_1' t}$$

- The procedure is continued for the number of desired terms, or until a required precision is reached

Frequency determination

- The accuracy of a simple FFT even for a simple sinusoidal signal is not better than $|\nu - \nu_T| = \dfrac{1}{T}$
- Calculating the Fourier integral explicitly

$$\phi(\omega) = < f(t),\ e^{i\omega t} > = \frac{1}{T}\int_0^T f(t)\ e^{-i\omega t}\ dt$$

shows that the maximum lies in between the main picks of the FFT

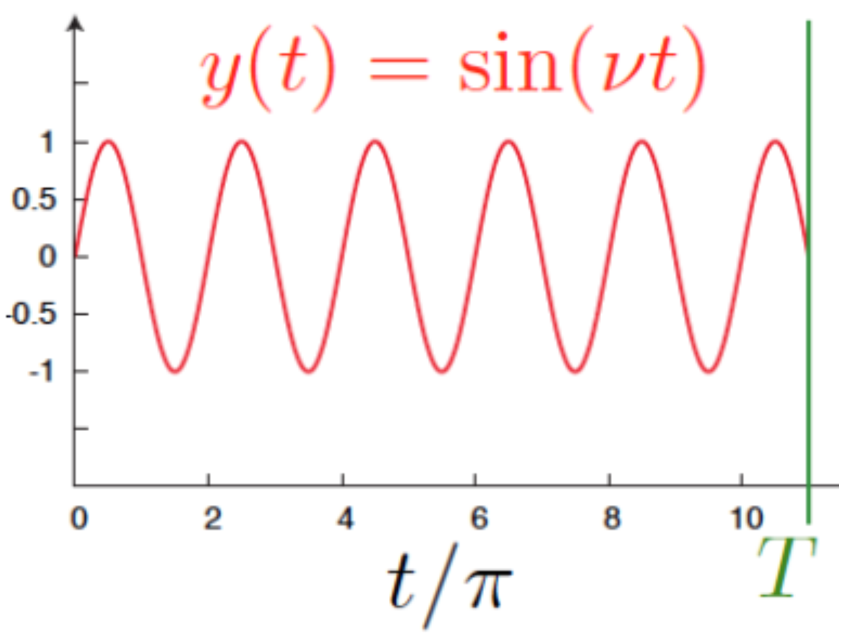

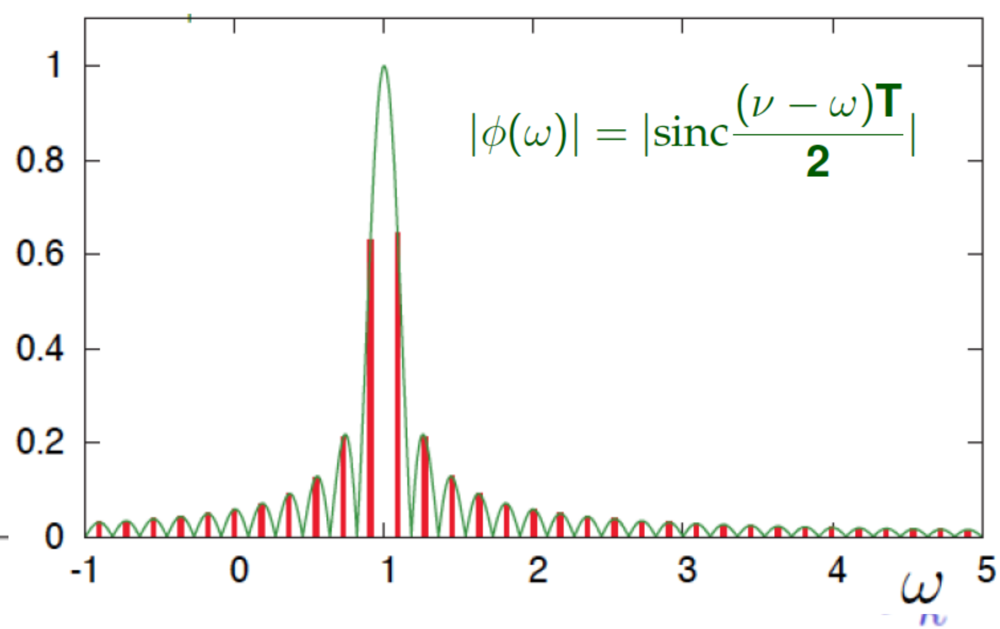

- A more complicated signal with two frequencies

$$f(t) = a_1 e^{i\omega_1 t} + a_2 e^{i\omega_2 t}$$

shifts slightly the maximum with respect to its real location

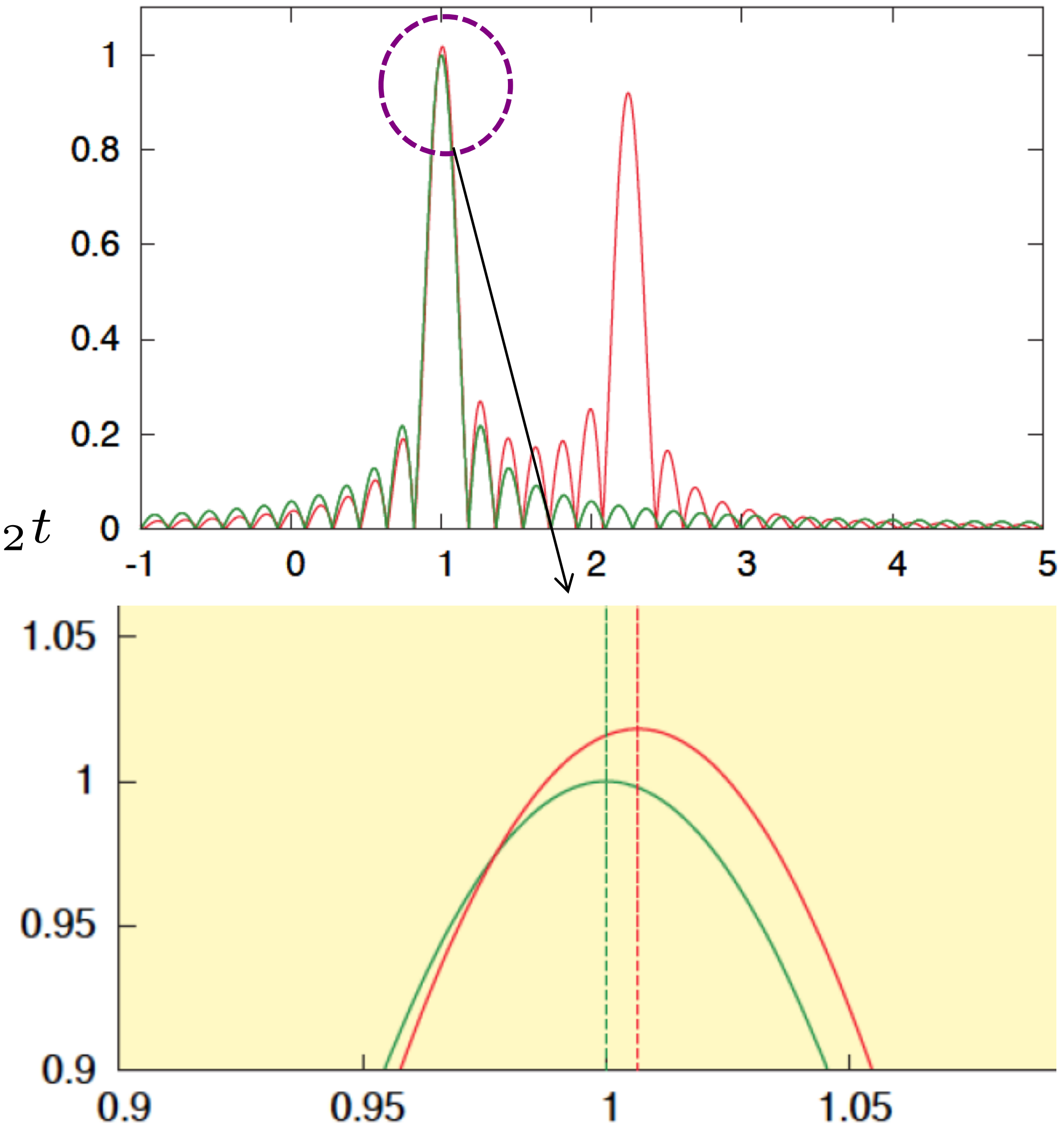

Window function

- A window function like the Hanning filter $\chi_1(t) = 1 + \cos(\pi t/T)$ kills side-lobs and allows a very accurate determination of the frequency

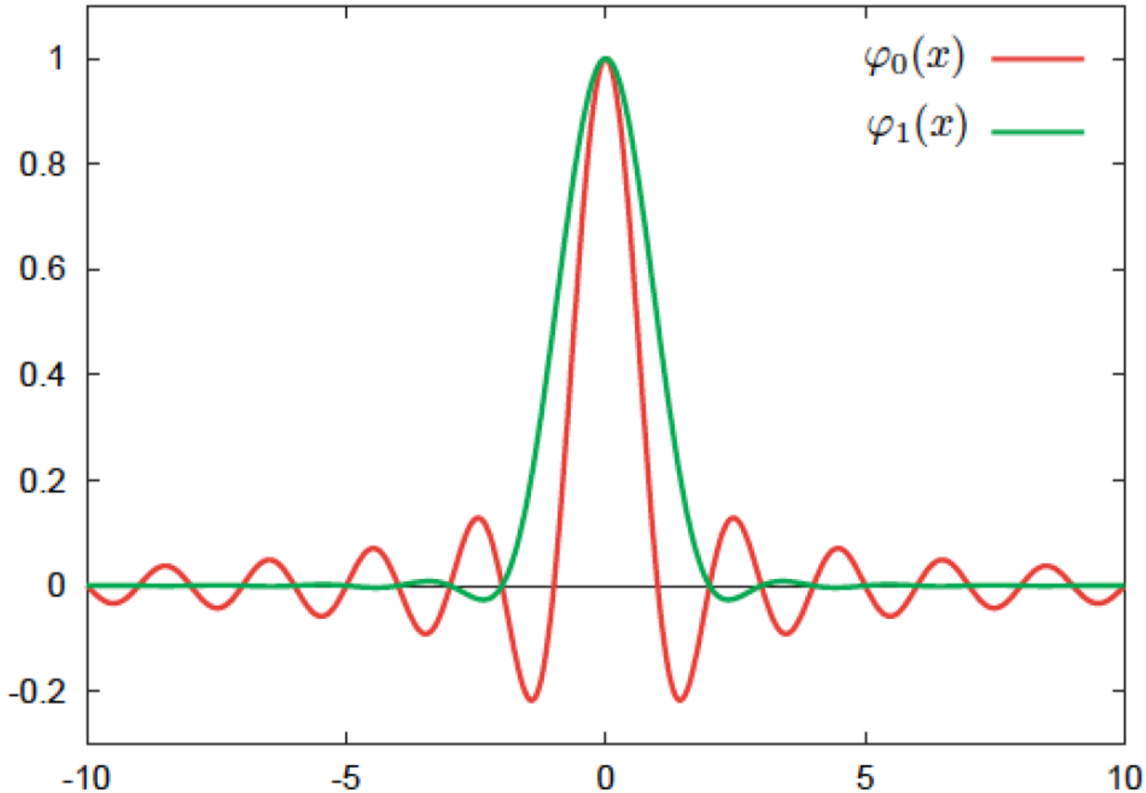

Precision of NAFF

- For a general window function of order p
$$\chi_p(t) = \frac{2^p (p!)^2}{(2p)!}(1+\cos \pi t)^p$$
Laskar (1996) proved a theorem stating that the solution provided by the NAFF algorithm converges asymptotically towards the real KAM quasi-periodic solution with precision
$$\nu_1 - \nu_1^T \propto \frac{1}{T^{2p+2}}$$
- In particular, for no filter (i.e. $p = 0$) the precision is $\frac{1}{T^2}$, whereas for the Hanning filter ($p = 1$), the precision is of the order of $\frac{1}{T^4}$

Aspects of the frequency map

- In the vicinity of a resonance the system behaves like a pendulum
- Passing through the elliptic point for a fixed angle, a fixed frequency (or rotation number) is observed
- Passing through the hyperbolic point, a frequency jump is oberved

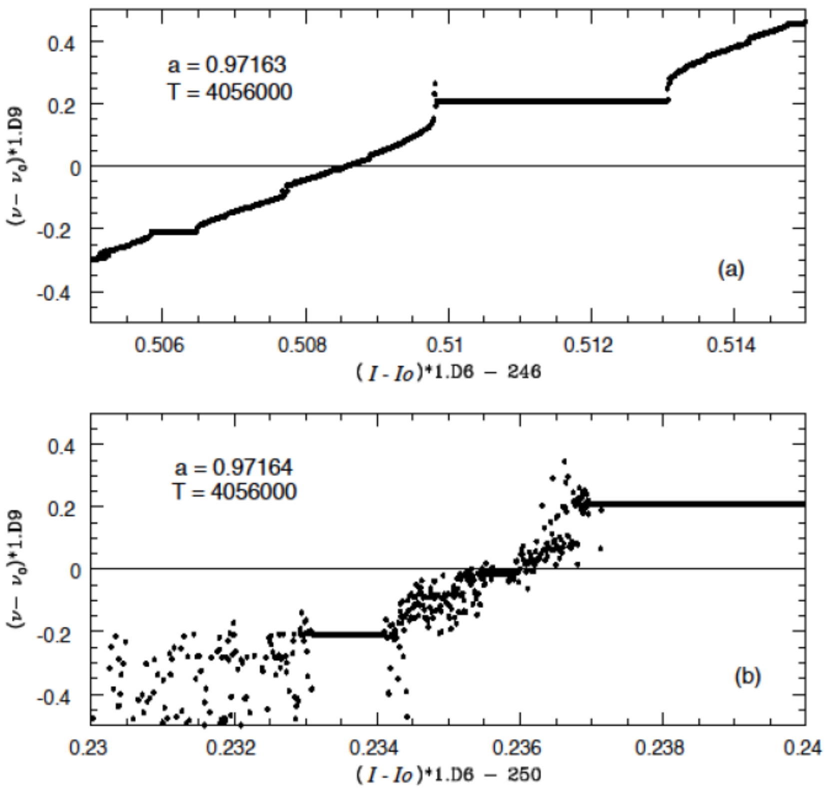

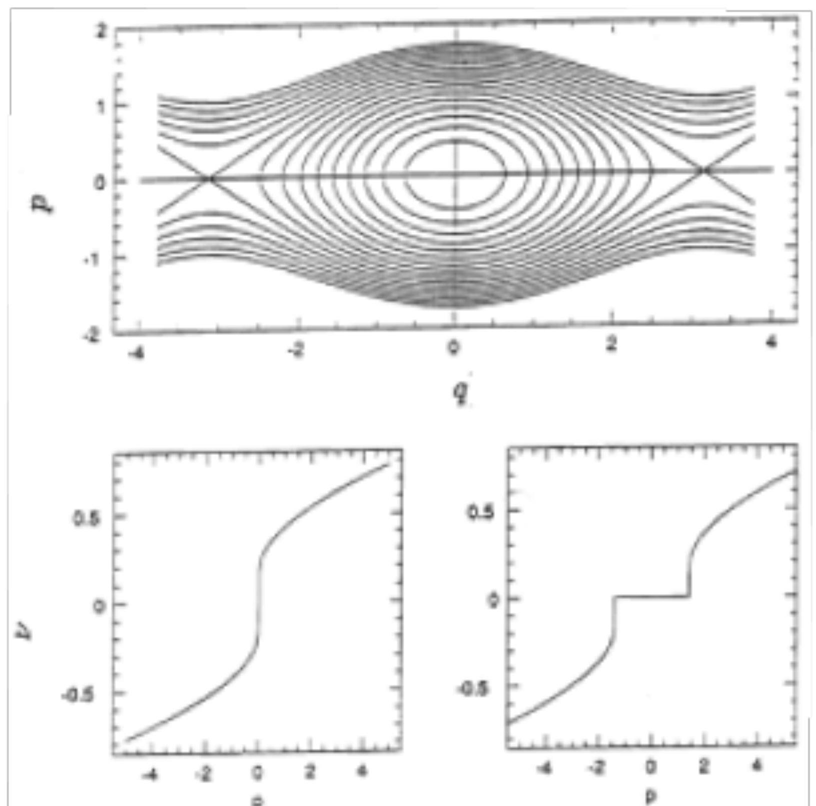

Diffusion in frequency space

- For a 2 degrees of freedom Hamiltonian system, the frequency space is a line, the tori are dots on this lines, and the chaotic zones are confined by the existing KAM tori
- For a system with 3 or more degrees of freedom, KAM tori are still represented by dots but do not prevent chaotic trajectories to diffuse

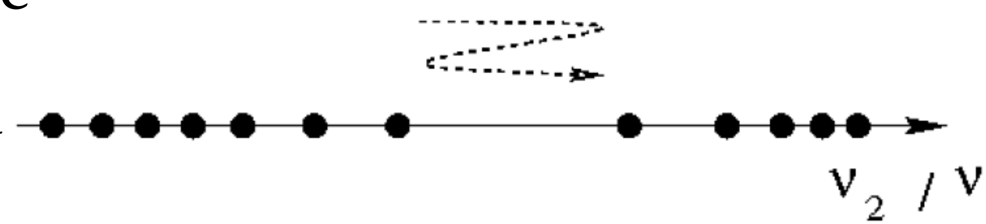

- This topological possibility of particles diffusing is called **Arnold diffusion**
- This diffusion is supposed to be extremely small in their vicinity, as tori act as effective barriers (**Nechoroshev theory**)

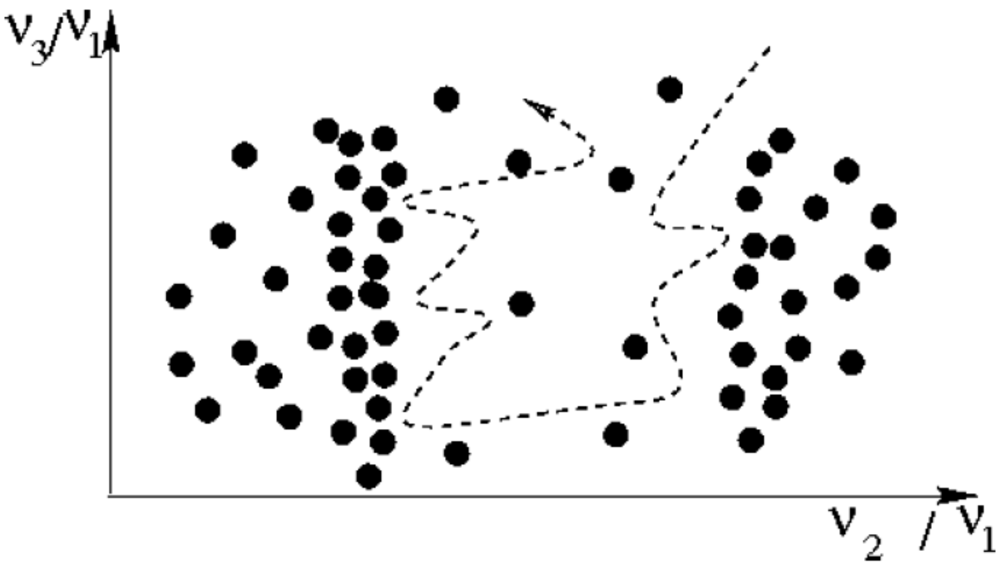

Building the frequency map

- Choose coordinates (x_i, y_i) with p_x and p_y=0
- Numerically integrate the phase trajectories through the lattice for sufficient number of turns
- Compute through NAFF Q_x and Q_y after sufficient number of turns
- Plot them in the tune diagram

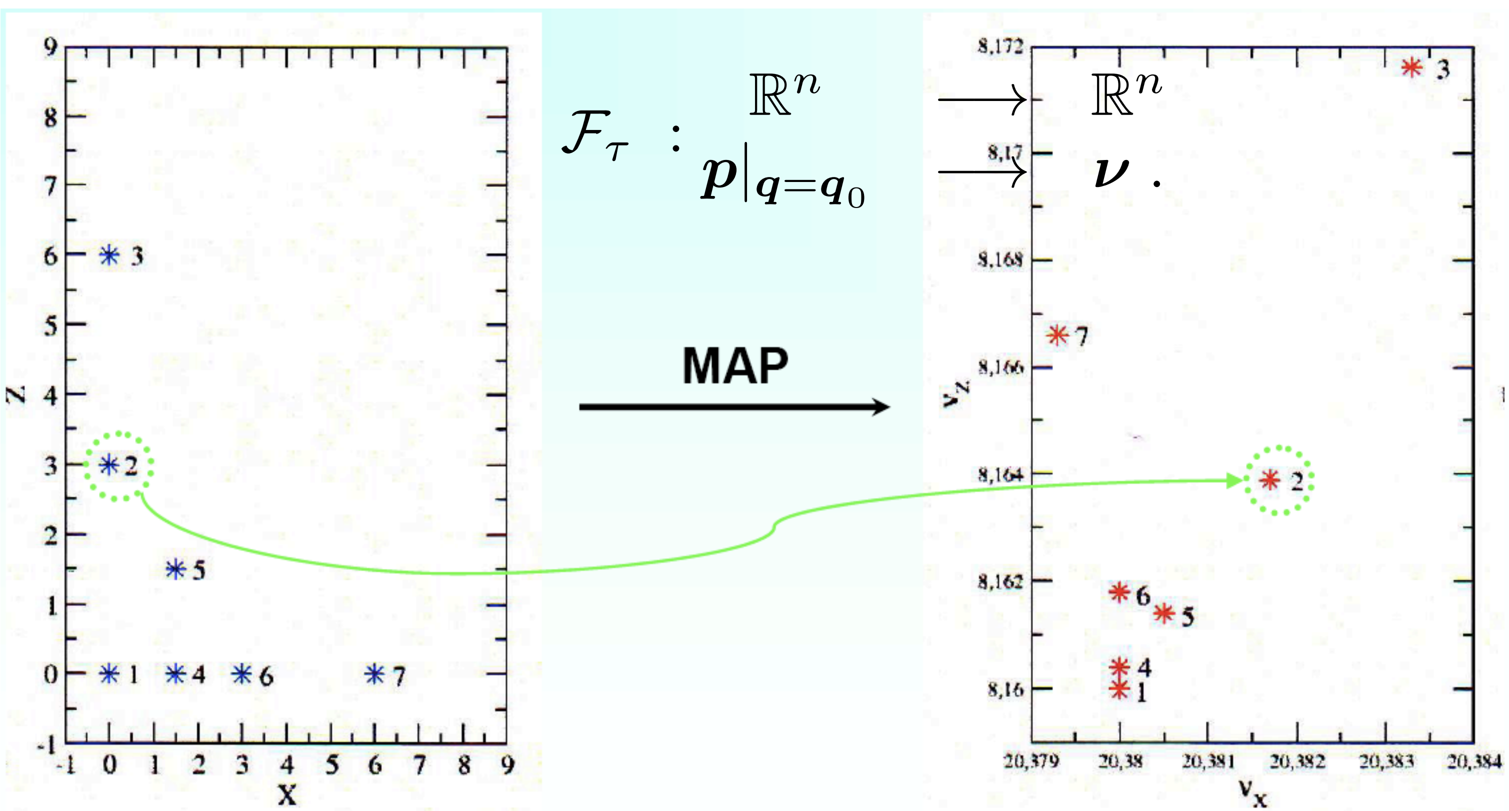

Contents of the 4th lecture

- Chaos detection methods and frequency map analysis
  - Dynamic aperture
  - Quasi-periodic motion
  - The NAFF algorithm
  - Frequency determination and precision
  - Aspects of frequency maps
- Simulation studies
  - Frequency and diffusion maps for the LHC
  - Beam-beam effect
  - Folded frequency maps
  - Magnet fringe-fields
  - Working point choice
  - Resonance free lattice
  - Symplectic integration
  - Correction schemes evaluation
- Experiments
  - Experimental frequency maps
  - Beam loss frequency maps
  - Space-charge frequency scan
- Summary

Frequency maps for the LHC

Y. Papaphilippou, PAC1999

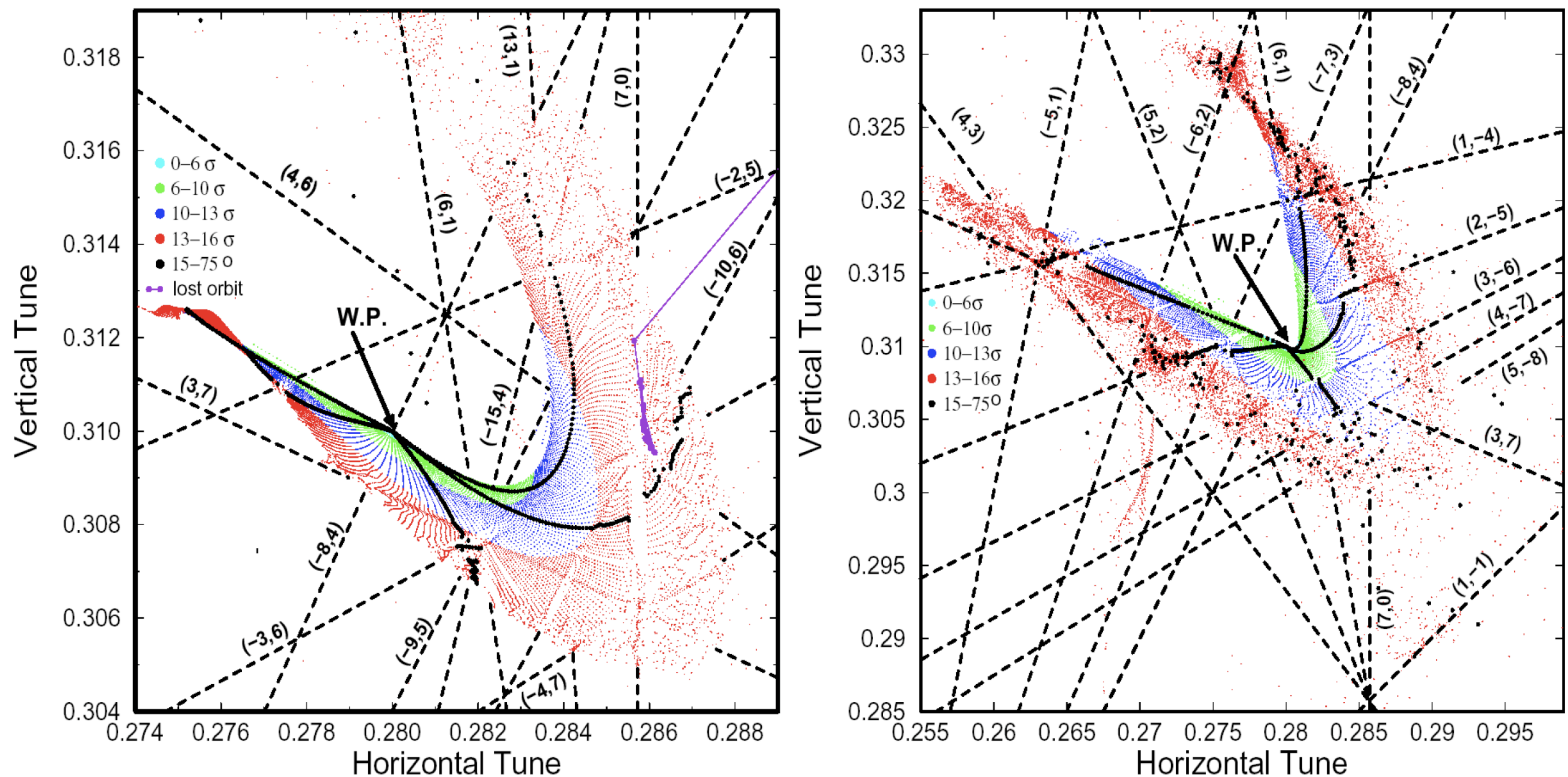

- Frequency maps for the target error table (left) and an increased random skew octupole error in the super-conducting dipoles (right)

Diffusion Maps

J. Laskar, PhysicaD, 1993

- Calculate frequencies for two equal and successive time spans and compute frequency diffusion vector:

$$\boldsymbol{D}\big|_{t=\tau} = \boldsymbol{\nu}\big|_{t\in(0,\tau/2]} - \boldsymbol{\nu}\big|_{t\in(\tau/2,\tau]}$$

- Plot the initial condition space color-coded with the norm of the diffusion vector
- Compute a diffusion quality factor by averaging all diffusion coefficients normalized with the initial conditions radius

$$D_{QF} = \left\langle \frac{|\boldsymbol{D}|}{(I_{x0}^2 + I_{y0}^2)^{1/2}} \right\rangle_R$$

Diffusion maps for the LHC

Y. Papaphilippou, PAC1999

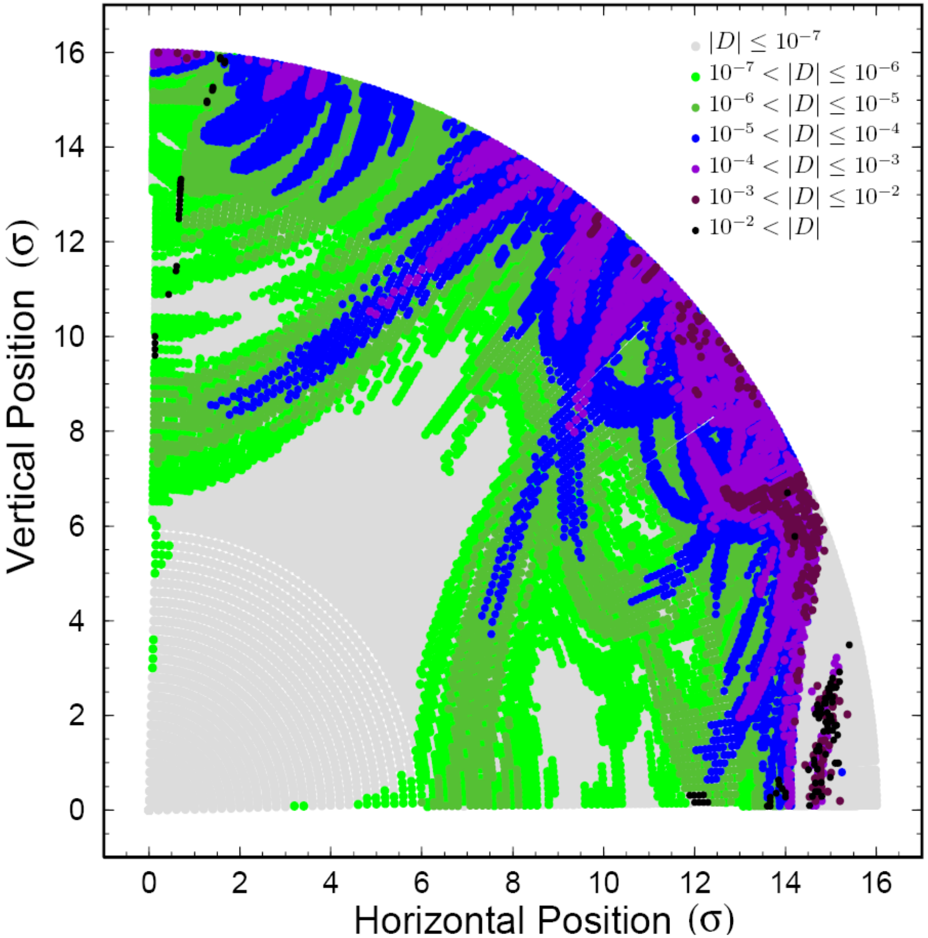

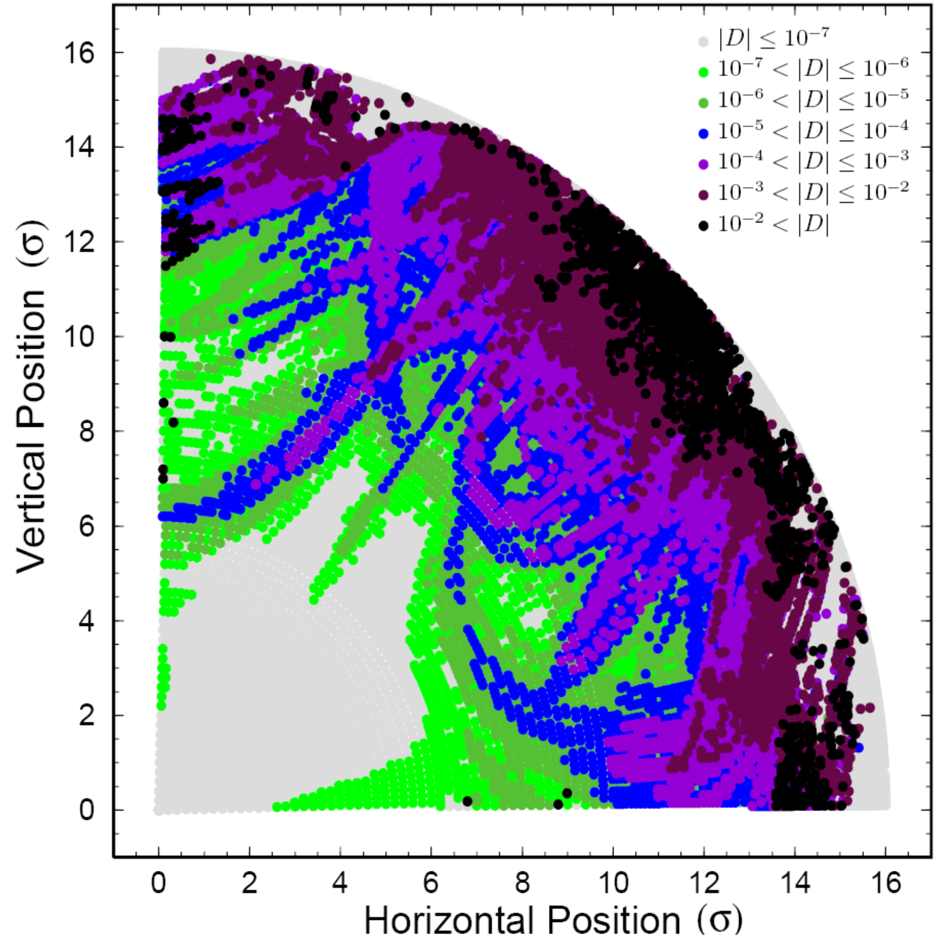

Diffusion maps for the target error table (left) and an increased random skew octupole error in the super-conducting dipoles (right)

Beam-Beam interaction

Variable	Symbol	Value
Beam energy	E	7 TeV
Particle species	$\cdots$	protons
Full crossing angle	θ_c	300 μrad
rms beam divergence	σ'_x	31.7 μrad
rms beam size	σ_x	15.9 μm
Normalized transv. rms emittance	$\gamma\varepsilon$	3.75 μm
IP beta function	β^*	0.5 m
Bunch charge	N_b	$(1 \times 10^{11} - 2 \times 10^{12})$
Betatron tune	Q_0	0.31

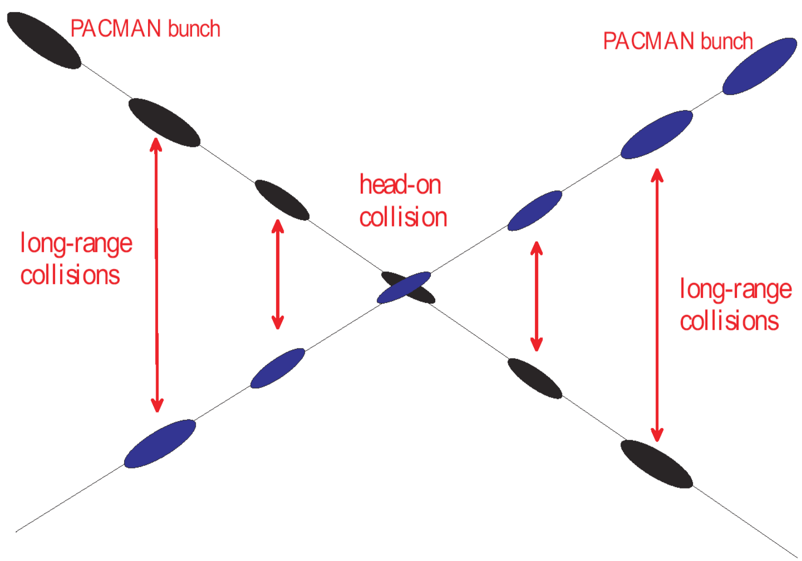

- Long range beam-beam interaction represented by a 4D kick-map

$$\Delta x = -\,n_{par}\,\frac{2r_pN_b}{\gamma}\left[\frac{x'+\theta_c}{\theta_t^2}\left(1-e^{-\frac{\theta_t^2}{2\theta_{x,y}^2}}\right) - \frac{1}{\theta_c}\left(1-e^{-\frac{\theta_c^2}{2\theta_{x,y}^2}}\right)\right]$$

$$\Delta y = -\,n_{par}\,\frac{2r_pN_b}{\gamma}\,\frac{y'}{\theta_t^2}\left(1-e^{-\frac{\theta_t^2}{2\theta_{x,y}^2}}\right)$$

with $$\theta_t \equiv \left((x'+\theta_c)^2 + {y'}^2\right)^{1/2}$$

Head-on vs Long range interaction

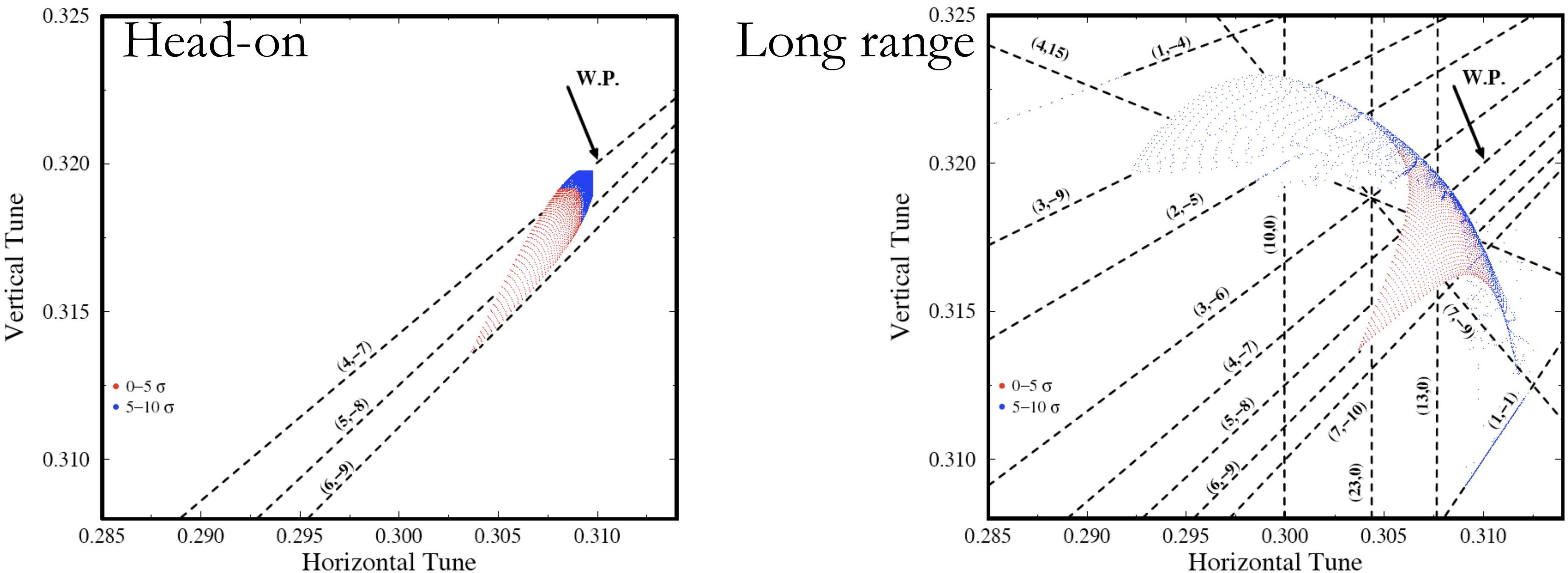

- Proved dominant effect of long range beam-beam effect
- Dynamic Aperture (around 6σ) located at the folding of the map (indefinite torsion)
- Dynamics dominated by the 1/r part of the force, reproduced by electrical wire, which was proposed for correcting the effect
- Experimental verification in SPS and installation to the LHC IPs

Action variance vs. frequency diffusion

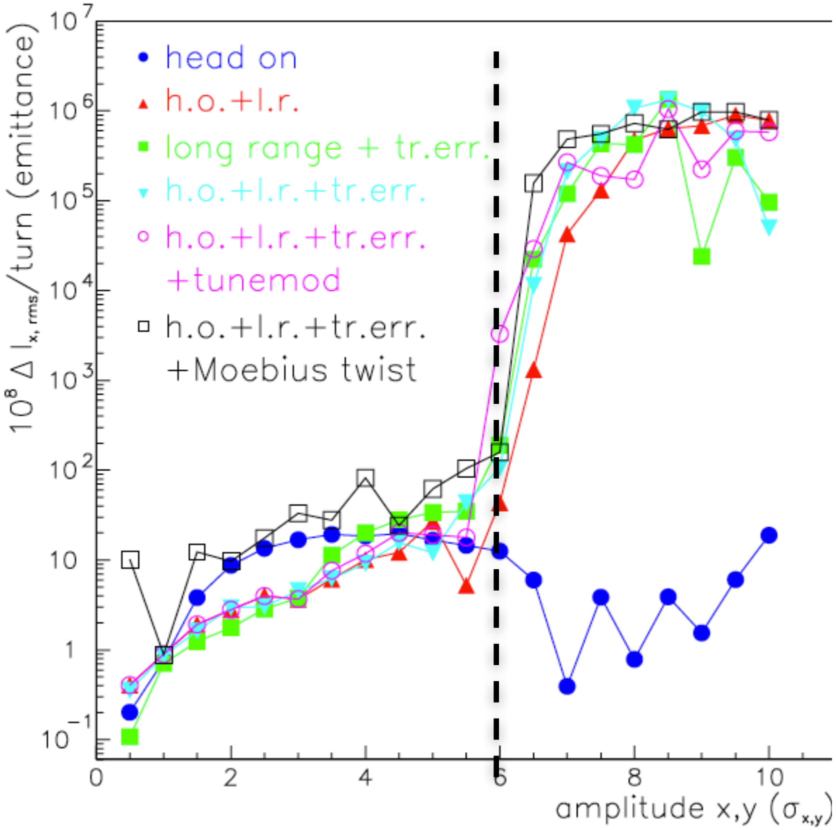

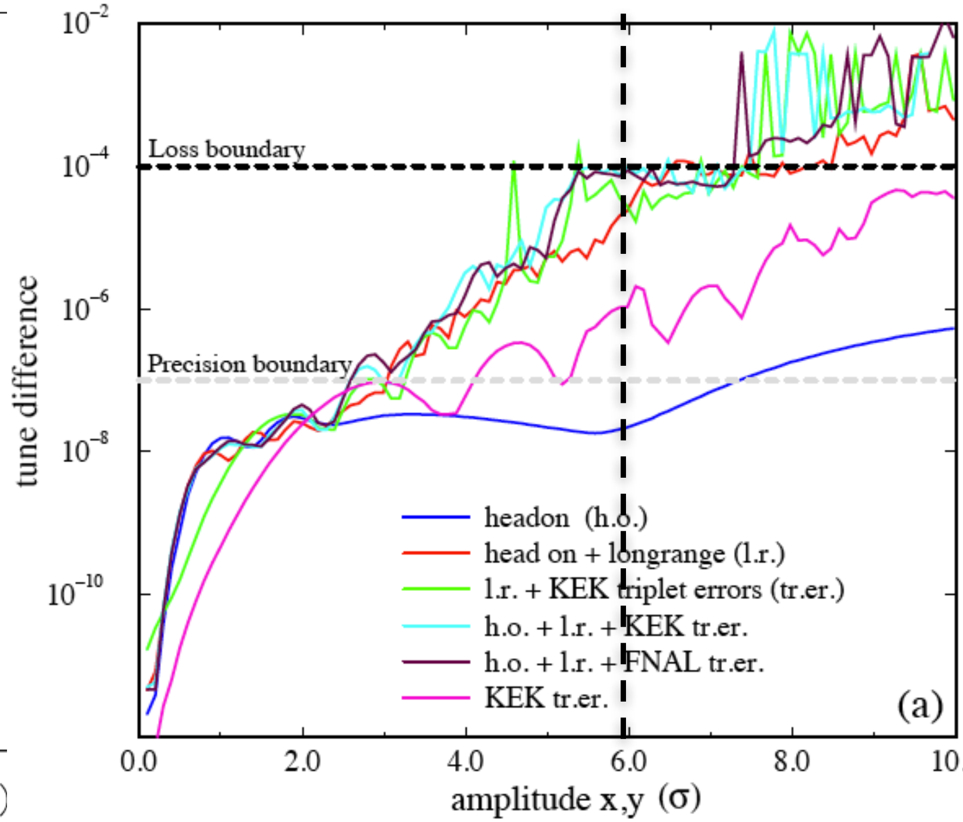

- Very good agreement of diffusive aperture boundary (action variance) with frequency variation (loss boundary corresponding to around 1 frequency unit change in 10^7 turns)

Folded frequency maps

- The torsion $M = \left(\frac{\partial \nu(I)}{\partial I}\right) = \left(\frac{\partial^2 H_0(I)}{\partial I^2}\right)$

  $\nu = \begin{pmatrix} \nu_1 \\ \nu_2 \end{pmatrix} = M \begin{pmatrix} I_1 \\ I_2 \end{pmatrix}$

  with Hamiltonian

$$H = \frac{1}{2} I^\tau M I + o(I^2) + O(\varepsilon)$$

- For a fixed energy value and even in the presence of chaos

  $I^\tau M I \approx 2h = Cte$ or $\nu^\tau M^{-1} \nu \approx 2h = Cte$

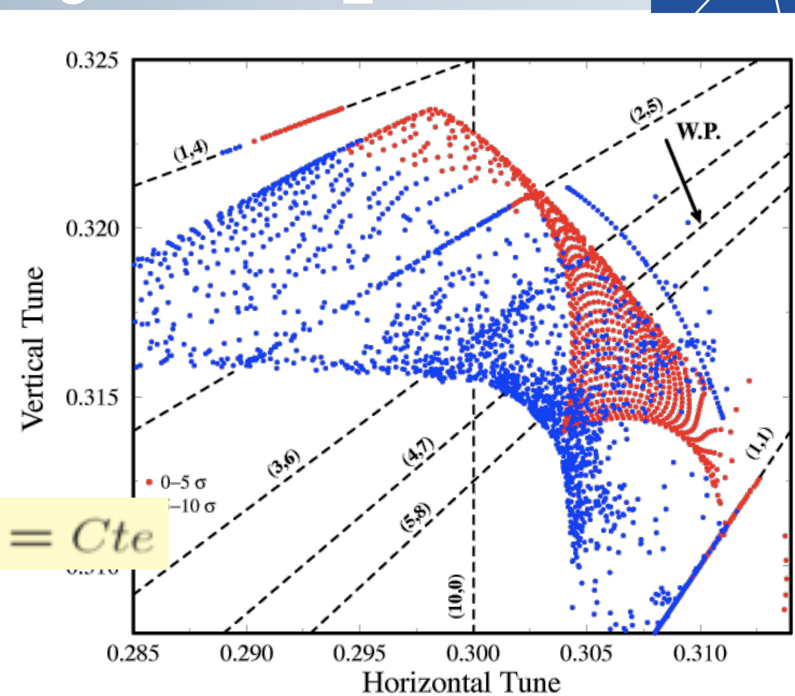

- For an accelerator $M^{-1} = \begin{pmatrix} a & c \\ c & b \end{pmatrix}$ is symmetric

no isotropic direction isotropic direction

$\det(M) > 0$

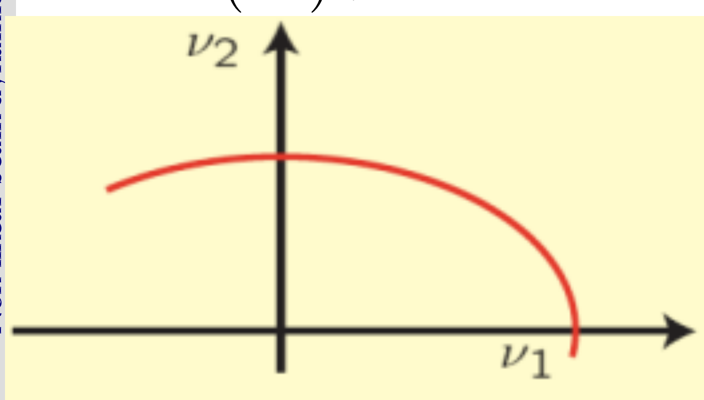

$\det(M) < 0$

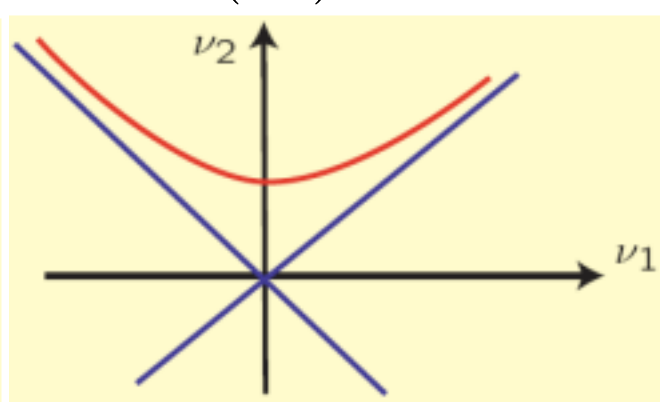

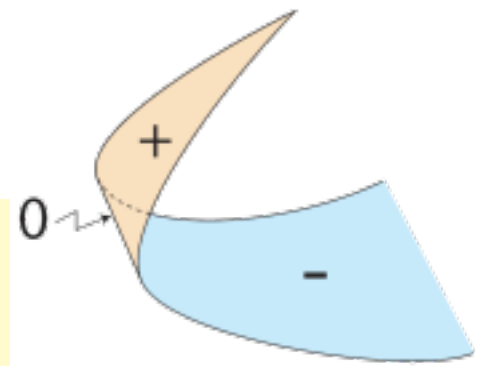

J.Laskar, PAC2003

Magnet fringe fields

- Up to now we considered only transverse fields
- Magnet fringe field is the longitudinal dependence of the field at the magnet edges
- Important when magnet aspect ratios and/or emittances are big

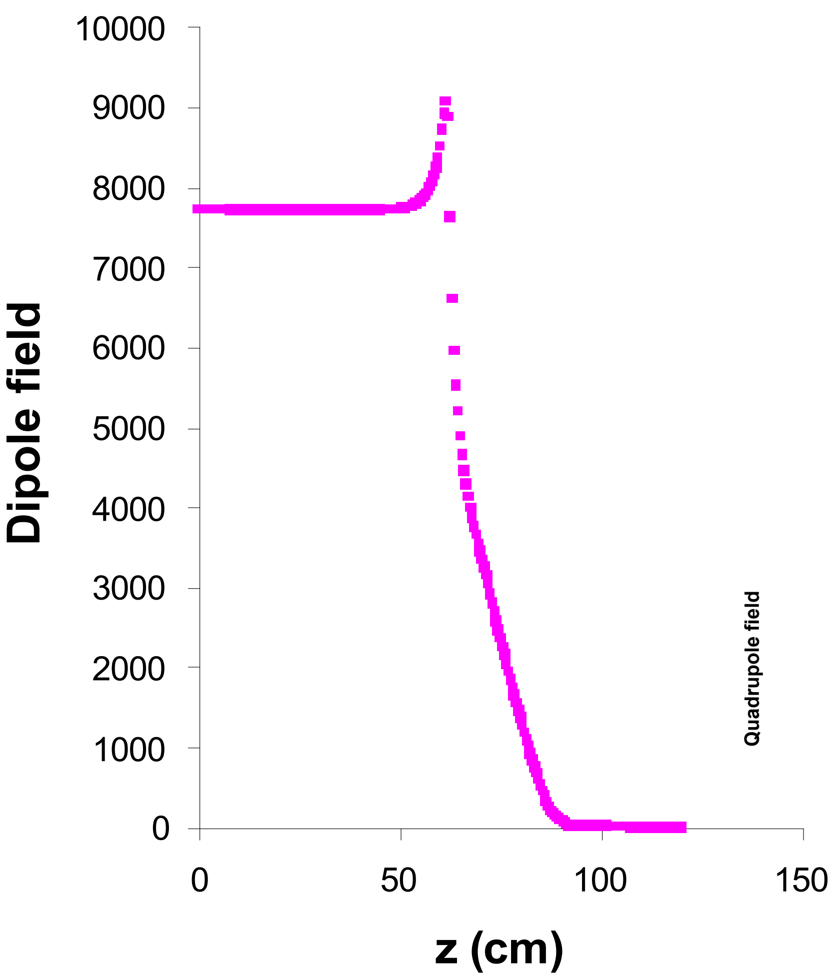

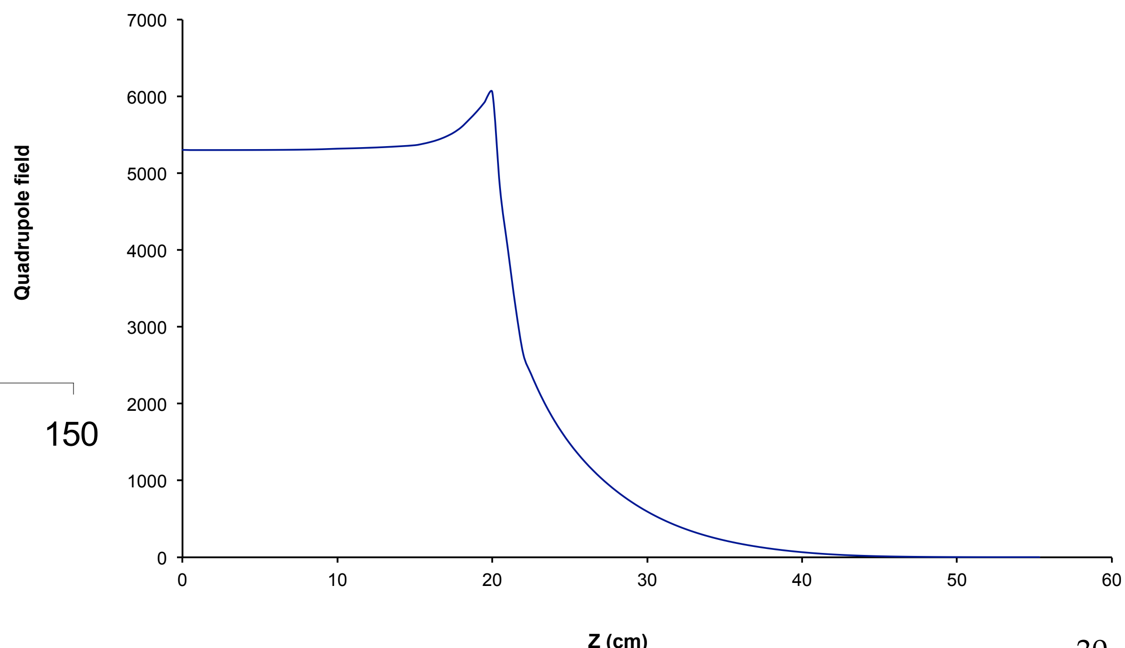

Quadrupole fringe field

General field expansion for a quadrupole magnet:

$$B_x = \sum_{m,n=0}^{\infty} \sum_{l=0}^{m} \frac{(-1)^m x^{2n} y^{2m+1}}{(2n)!(2m+1)!} \binom{m}{l} b^{[2l]}_{2n+2m+1-2l}$$

$$B_y = \sum_{m,n=0}^{\infty} \sum_{l=0}^{m} \frac{(-1)^m x^{2n+1} y^{2m}}{(2n+1)!(2m)!} \binom{m}{l} b^{[2l]}_{2n+2m+1-2l} \quad .$$

$$B_z = \sum_{m,n=0}^{\infty} \sum_{l=0}^{m} \frac{(-1)^m x^{2n+1} y^{2m+1}}{(2n+1)!(2m+1)!} \binom{m}{l} b^{[2l+1]}_{2n+2m+1-2l}$$

and to leading order

$$\begin{aligned} B_x &= y\left[b_1 - \frac{1}{12}(3x^2 + y^2) b_1^{[2]}\right] + O(5) \\ B_y &= x\left[b_1 - \frac{1}{12}(3y^2 + x^2) b_1^{[2]}\right] + O(5) \\ B_z &= xy b_1^{[1]} + O(4) \end{aligned}$$

The quadrupole fringe to leading order has an octupole-like effect

Magnet fringe fields

- From the hard-edge Hamiltonian

$$H_f = \frac{\pm Q}{12B\rho(1+\frac{\delta p}{p})}(y^3 p_y - x^3 p_x + 3x^2 y p_y - 3y^2 x p_x),$$

the first order shift of the frequencies with amplitude can be computed analytically

$$\begin{pmatrix} \delta\nu_x \\ \delta\nu_y \end{pmatrix} = \begin{pmatrix} a_{hh} & a_{hv} \\ a_{hv} & a_{vv} \end{pmatrix} \begin{pmatrix} 2J_x \\ 2J_y \end{pmatrix},$$

with the "anharmonicity" coefficients (torsion)

$$a_{hh} = \frac{-1}{16\pi B\rho} \sum_i \pm Q_i \beta_{xi} \alpha_{xi}$$
$$a_{hv} = \frac{1}{16\pi B\rho} \sum_i \pm Q_i (\beta_{xi}\alpha_{yi} - \beta_{yi}\alpha_{xi})$$
$$a_{vv} = \frac{1}{16\pi B\rho} \sum_i \pm Q_i \beta_{yi} \alpha_{yi}$$

Tune footprint for the SNS based on hard-edge (red) and realistic (blue) quadrupole fringe-field

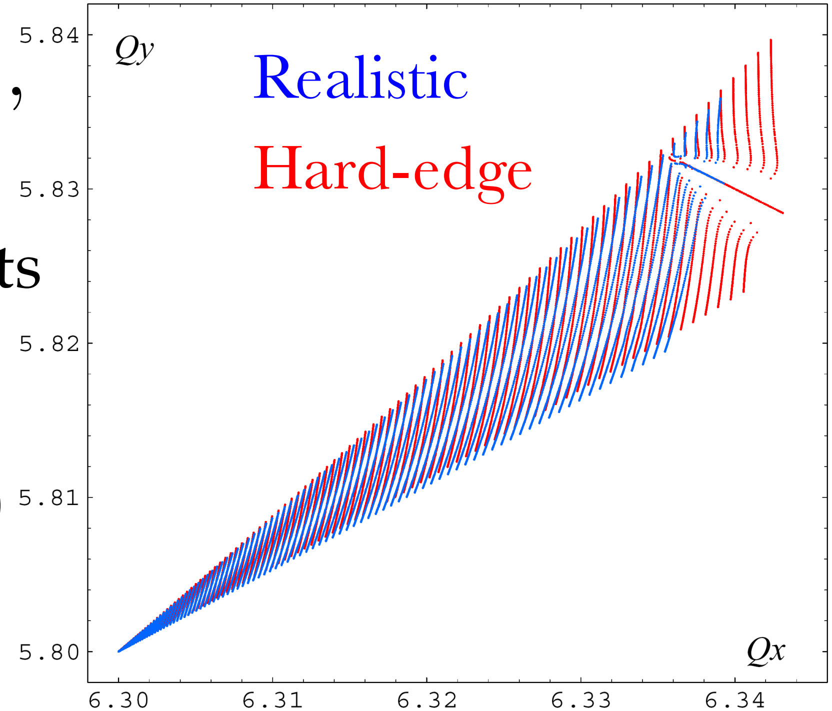

Off-momentum frequency maps

SNS Working Point $(Q_x,Q_y)=(6.4,6.3)$

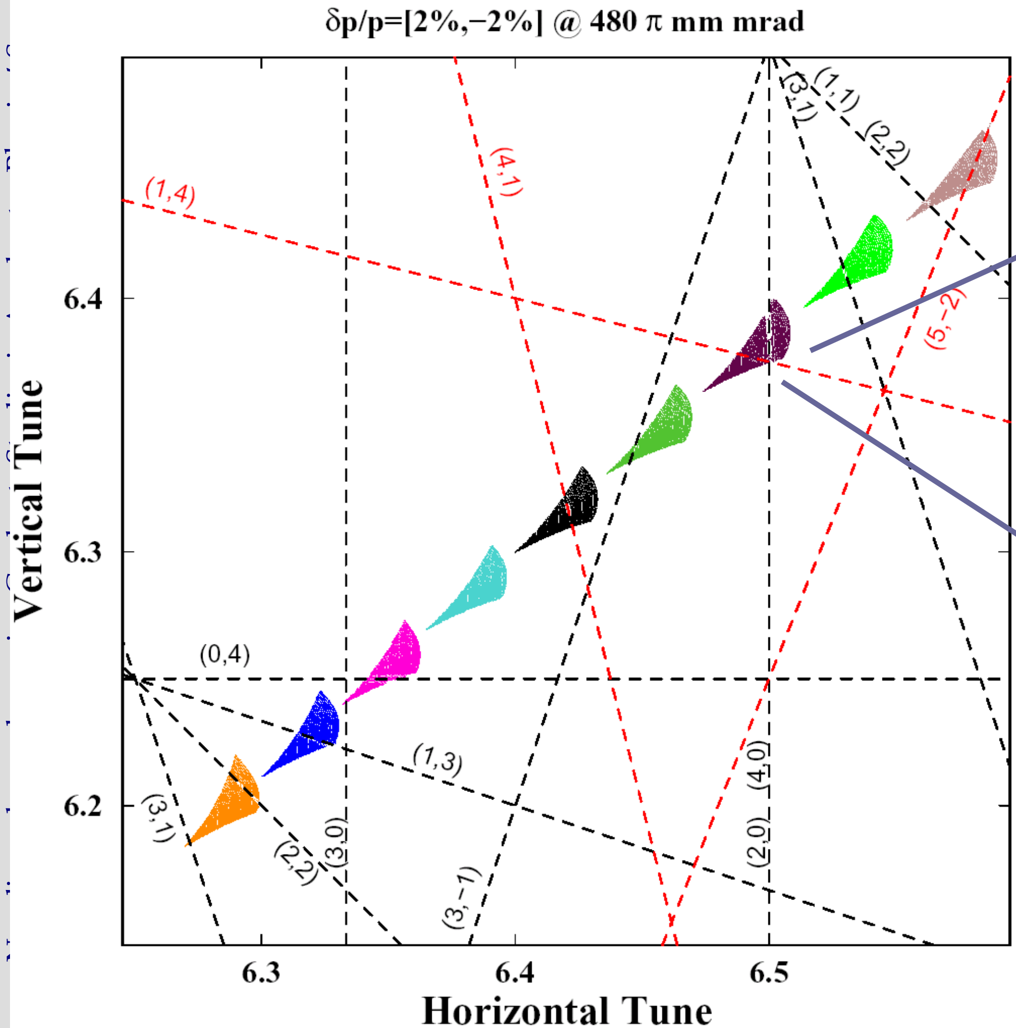

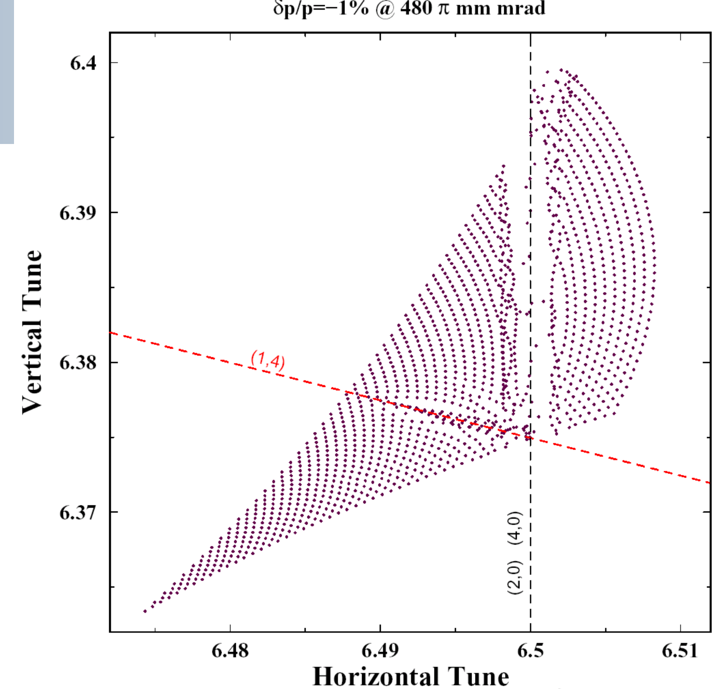

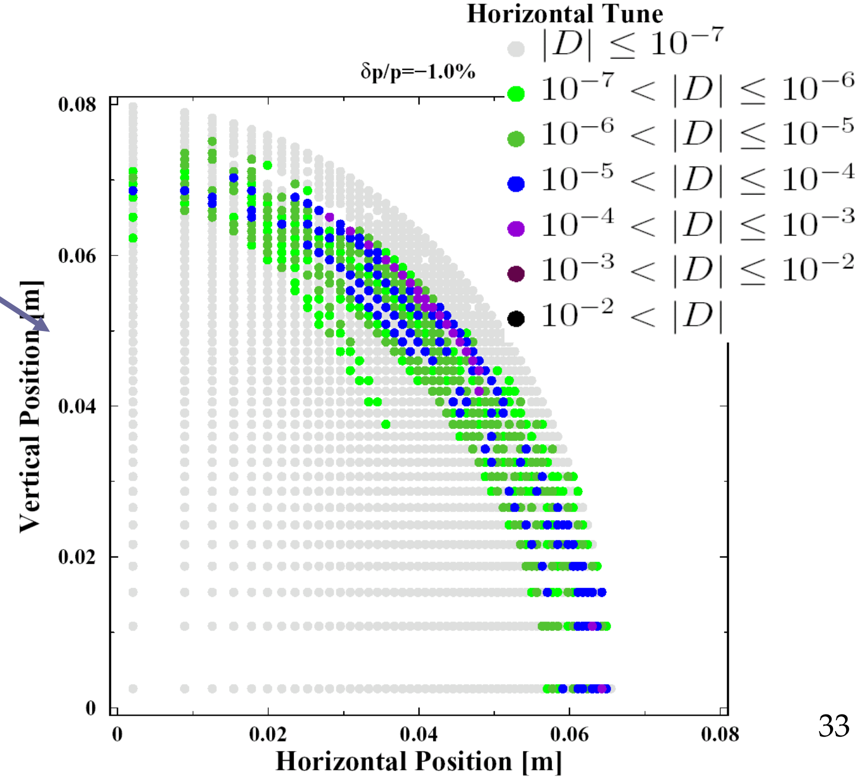

Choice of the SNS ring working point

Tune Diffusion quality factor

$$D_{QF} = \left\langle \frac{|\boldsymbol{D}|}{(I_{x0}^2 + I_{y0}^2)^{1/2}} \right\rangle_R$$

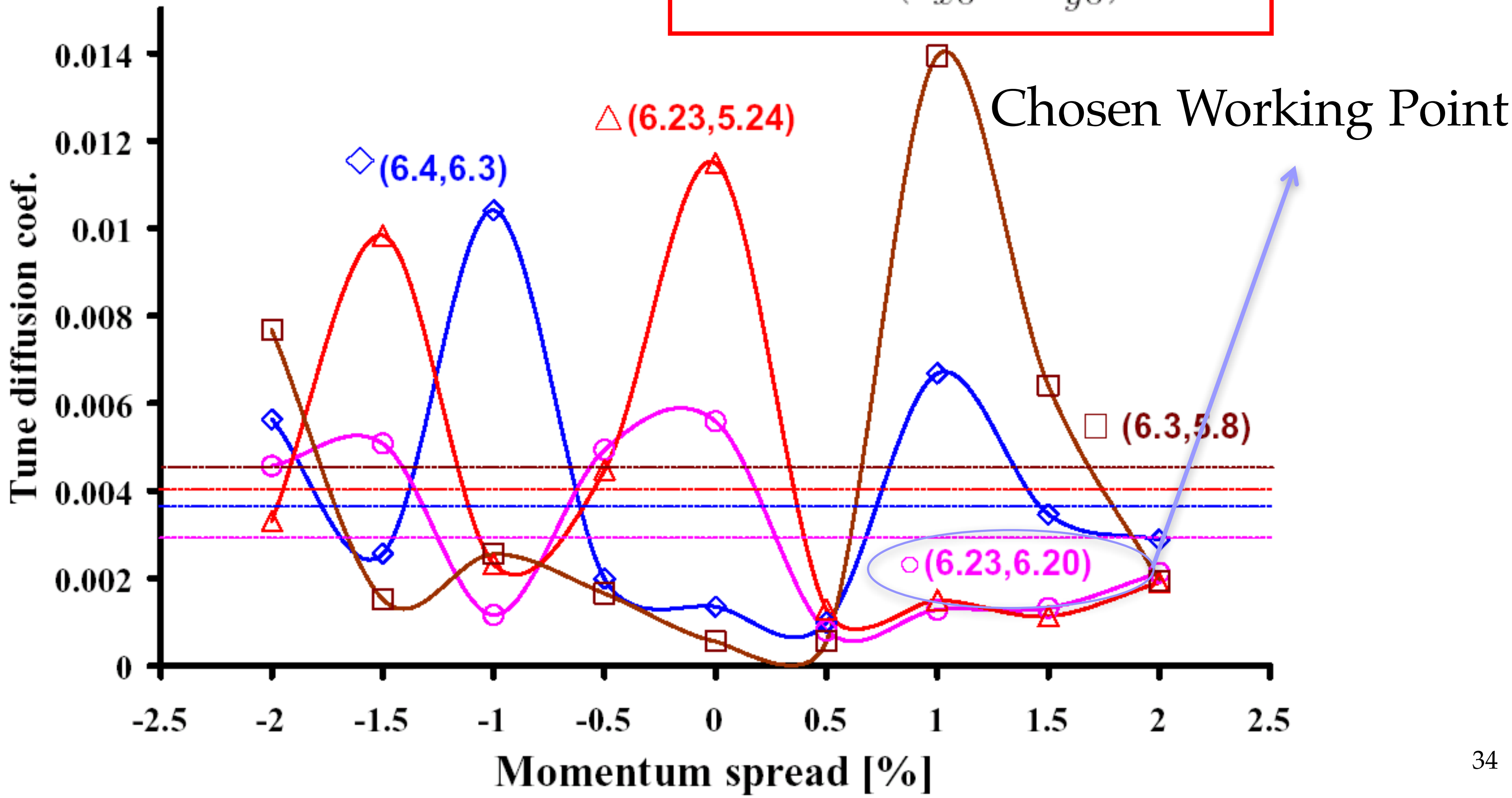

Correction schemes efficiency

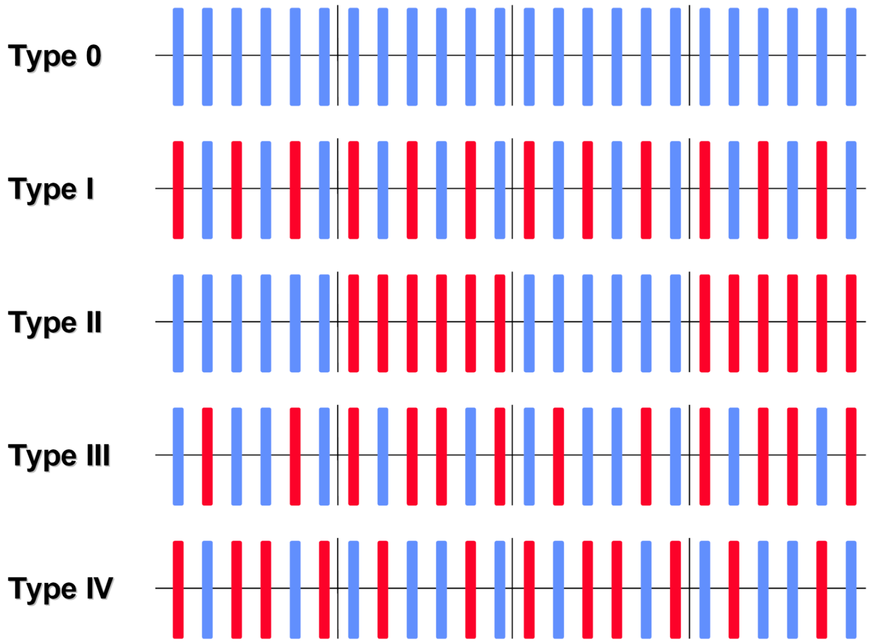

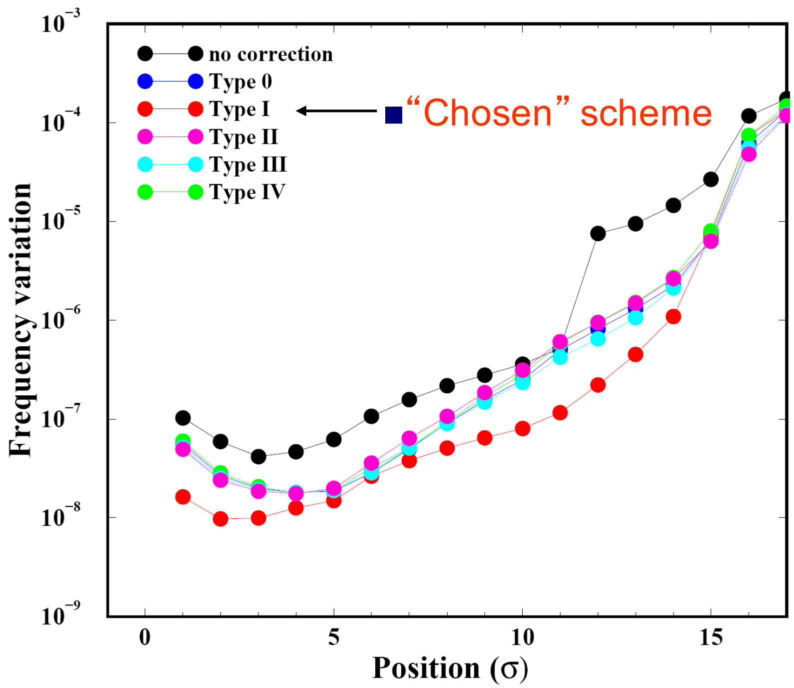

- Comparison of correction schemes for b_4 and b_5 errors in the LHC dipoles
- Frequency maps, resonance analysis, tune diffusion estimates, survival plots and short term tracking, proved that only half of the correctors are needed

Working point choice for SUPERB

- Figure of merit for choosing best working point is sum of diffusion rates with a constant added for every lost particle
- Each point is produced after tracking 100 particles
- Nominal working point had to be moved towards "blue" area

$$e^D = \sqrt{\frac{(\nu_{x,1}-\nu_{x,2})^2+(\nu_{y,1}-\nu_{y,2})^2}{N/2}}$$

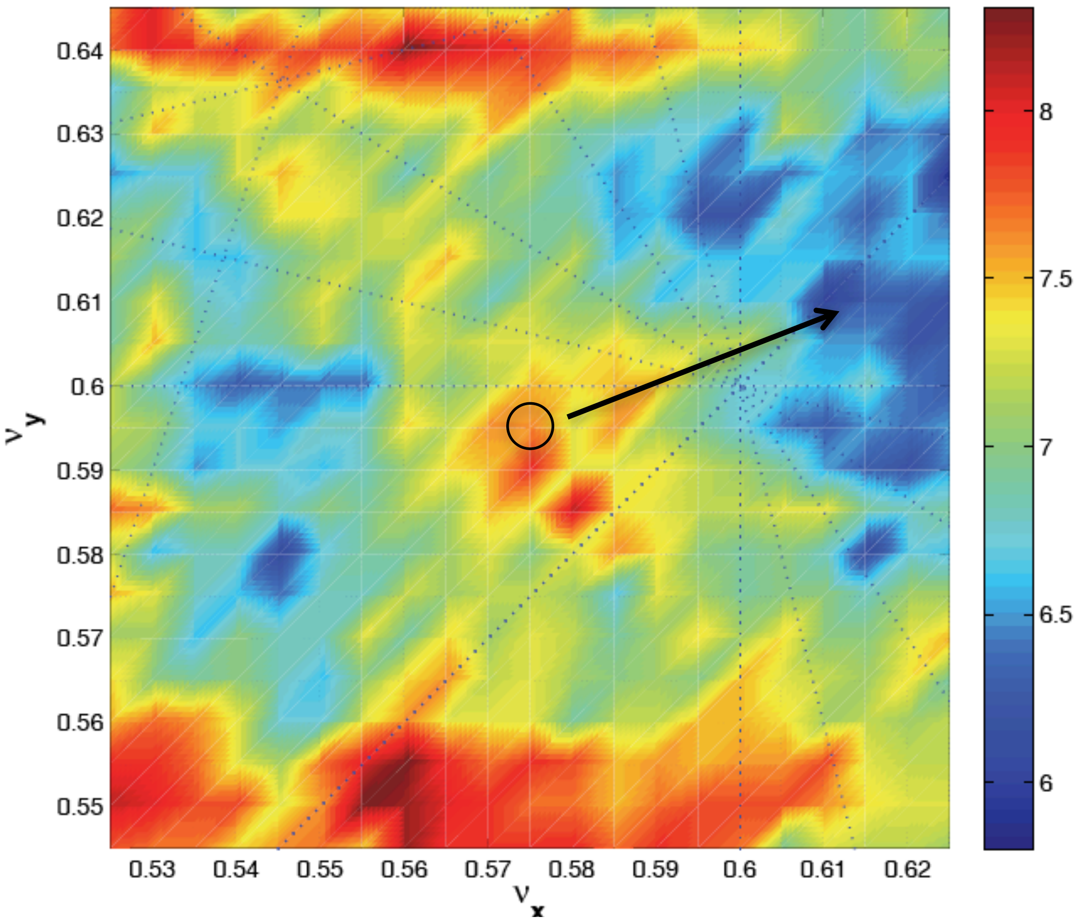

$$WPS = 0.1N_{lost} + \sum e^D$$

Application of the $SABA_2C$ integrator

- The one kick integrator reveals a completely different dynamics then the 10-kick
- $SABA_2C$ integrator captures the correct dynamics

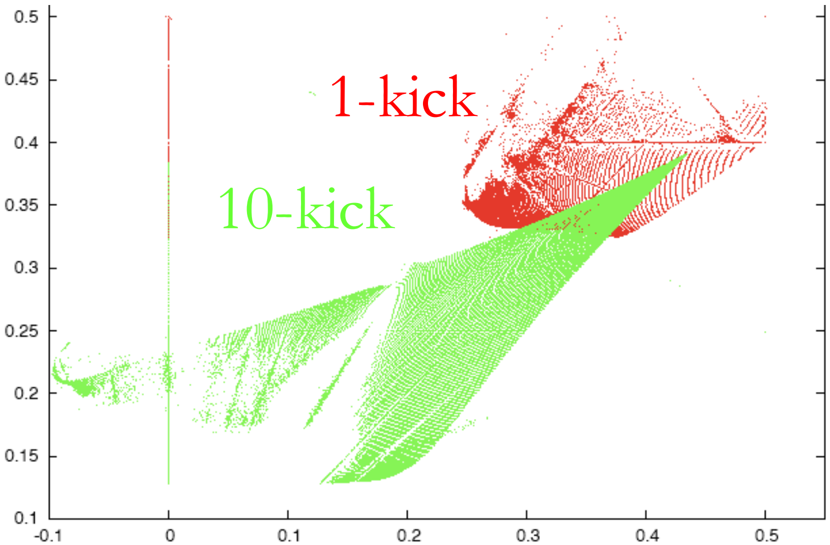

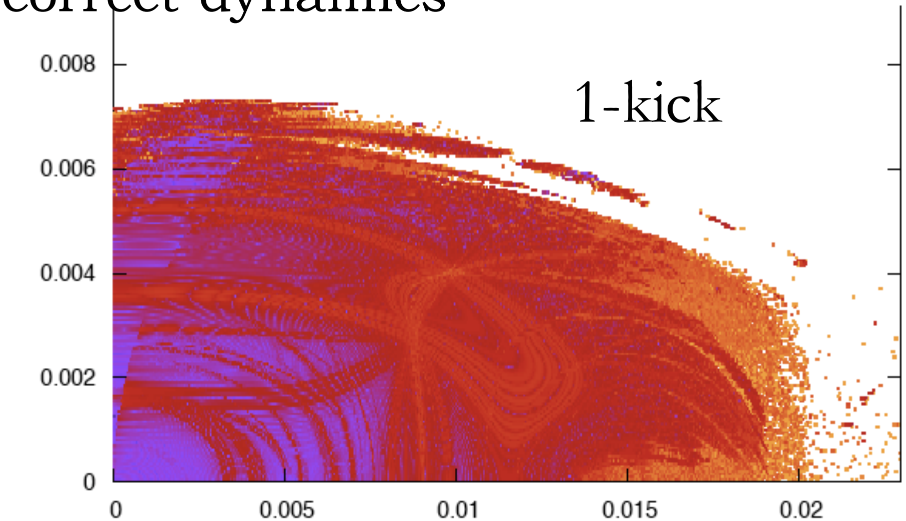

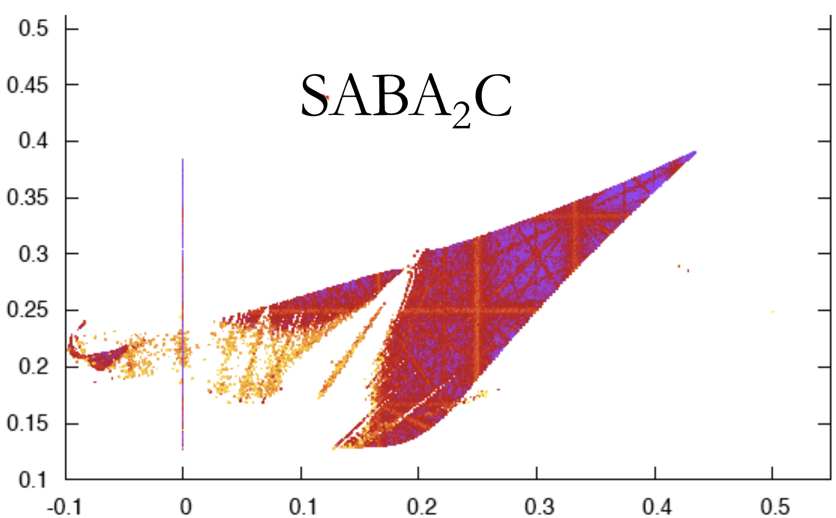

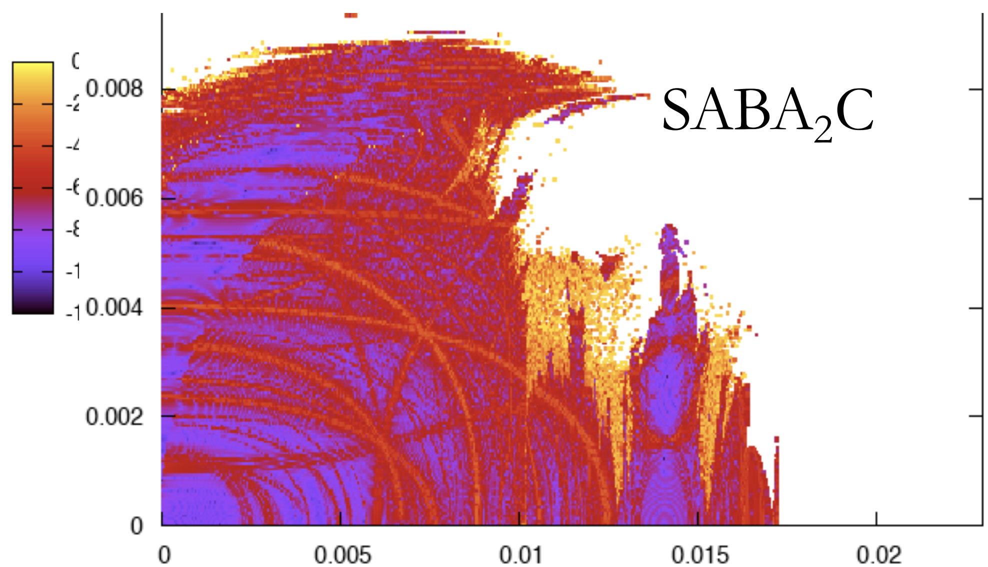

Resonance free lattice for CLIC PDR

- Non linear optimization based on phase advance scan for minimization of resonance driving terms and tune-shift with amplitude

$$\left|\sum_{p=0}^{N_c-1} e^{ip(n_x\mu_{x,c}+n_y\mu_{y,c})}\right| = \sqrt{\frac{1-\cos\left[N_c(n_x\mu_{x,c}+n_y\mu_{y,c})\right]}{1-\cos(n_x\mu_{x,c}+n_y\mu_{y,c})}} = 0$$

$$\Downarrow$$

$$N_c(n_x\mu_{x,c}+n_y\mu_{y,c}) = 2k\pi$$

$$n_x\mu_{x,c}+n_y\mu_{y,c} \neq 2k'\pi$$

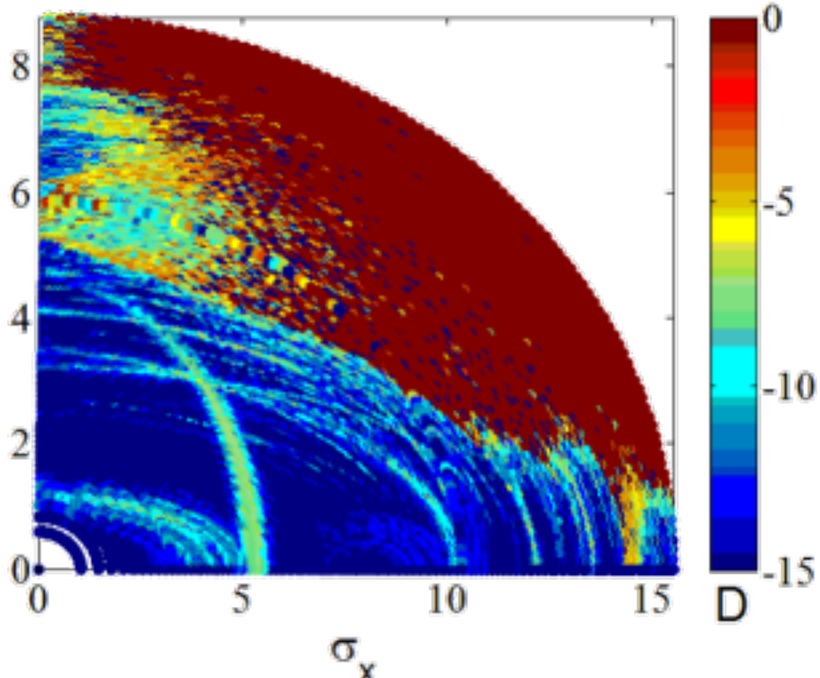

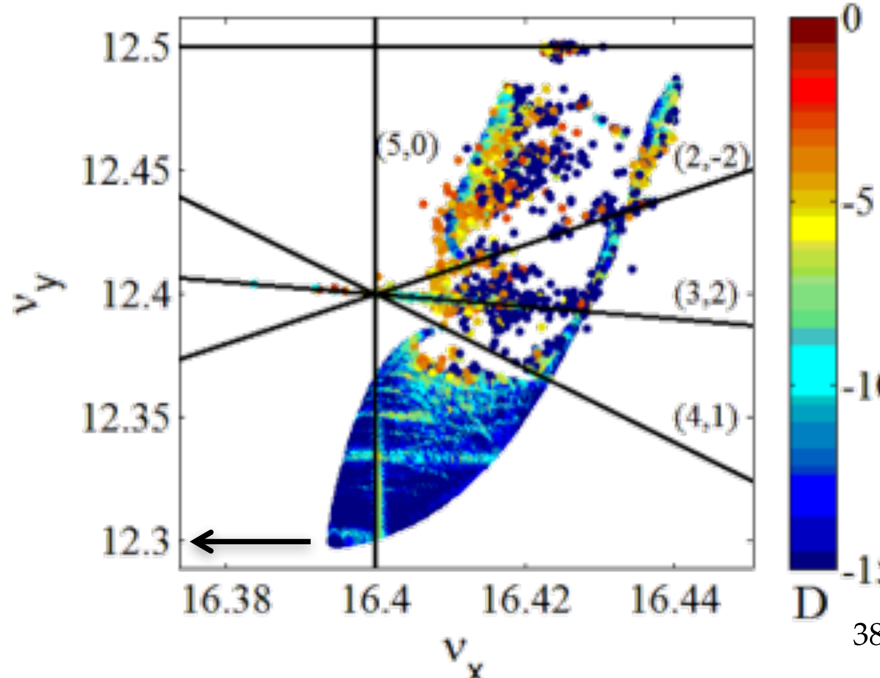

CERN PS2 sextupole scheme optimization

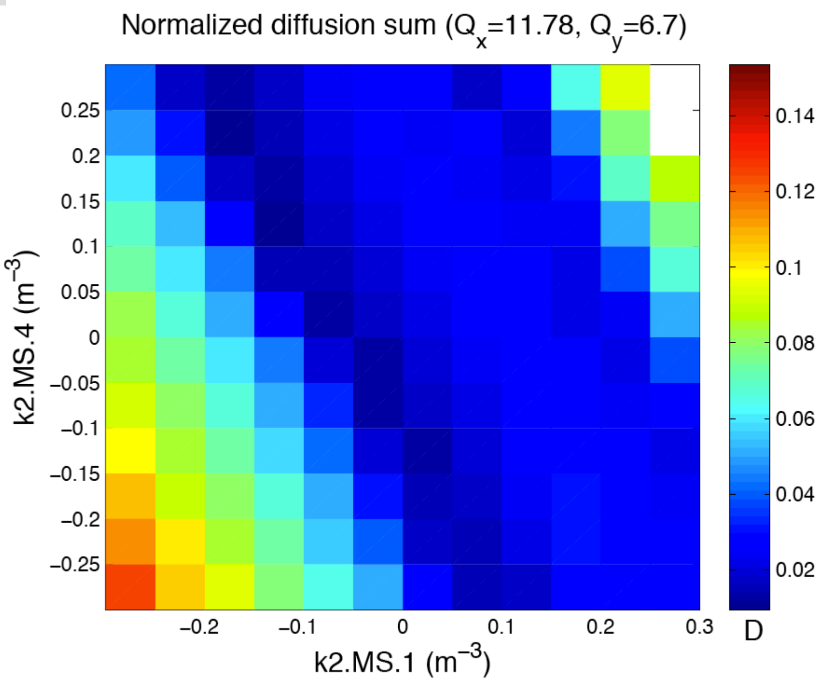

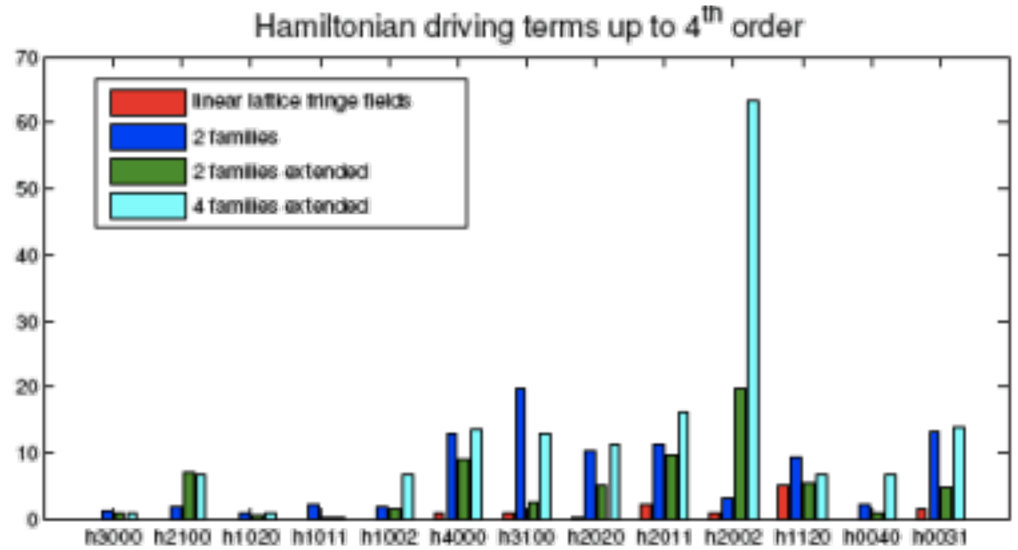

- Comparing different chromaticity sextupole correction schemes and working point optimization using normal form analysis, frequency maps and finally particle tracking
- Finding the adequate sextupole strengths through the tune diffusion coefficient

Contents of the 4th lecture

- Chaos detection methods and frequency map analysis
  - Dynamic aperture
  - Quasi-periodic motion
  - The NAFF algorithm
  - Frequency determination and precision
  - Aspects of frequency maps
- Simulation studies
  - Frequency and diffusion maps for the LHC
  - Beam-beam effect
  - Folded frequency maps
  - Magnet fringe-fields
  - Working point choice
  - Resonance free lattice
  - Symplectic integration
  - Correction schemes evaluation
- Experiments
  - Experimental frequency maps
  - Beam loss frequency maps
  - Space-charge frequency scan
- Summary

Experimental frequency maps

D. Robin, C. Steier, J. Laskar, and L. Nadolski, PRL 2000

- Frequency analysis of turn-by-turn data of beam oscillations produced by a fast kicker magnet and recorded on a Beam Position Monitors
- Reproduction of the non-linear model of the Advanced Light Source storage ring and working point optimization for increasing beam lifetime

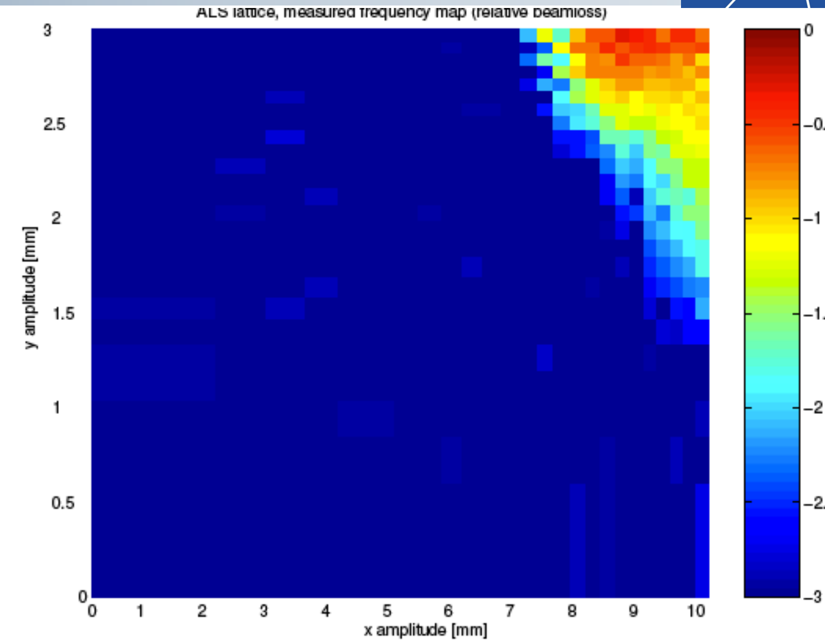

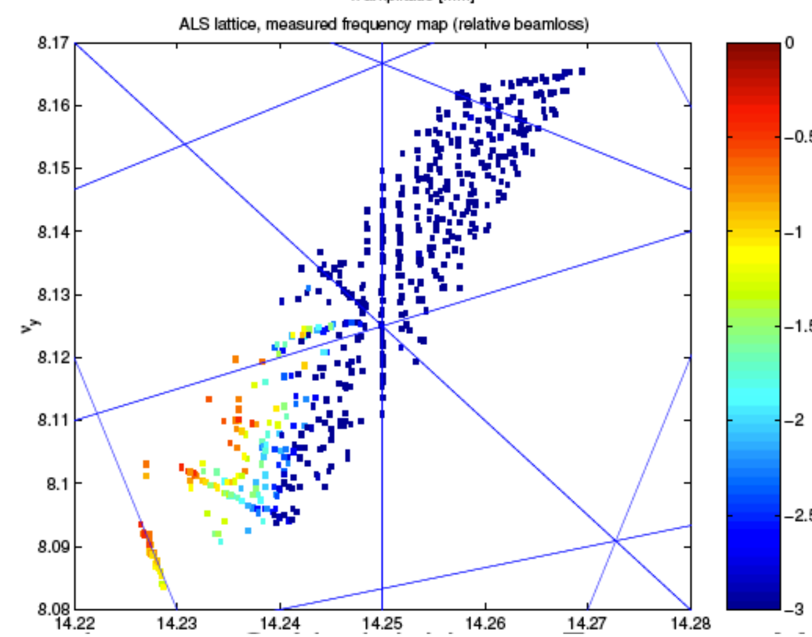

Beam loss frequency maps in the SPS

- Strength of resonance lines identified by derivative of beam intensity (average beam loss rate)
- Tunes continuously monitored using NAFF and beam intensity recorded with current transformer

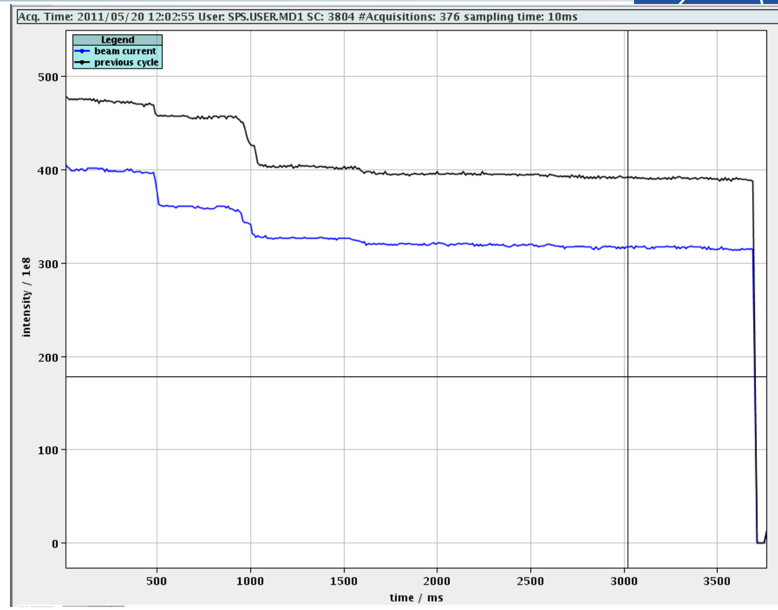

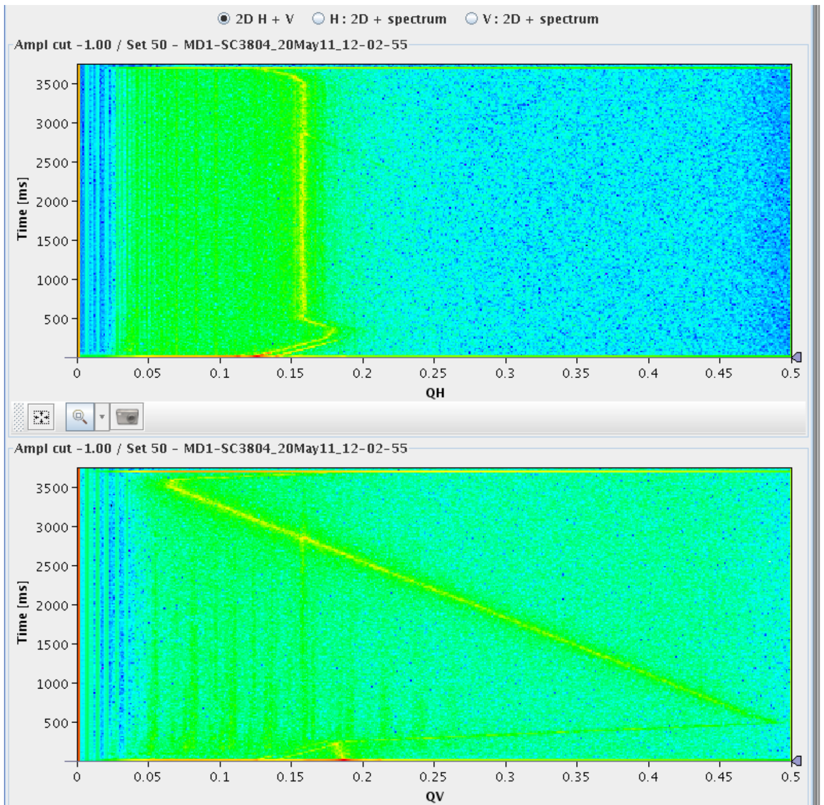

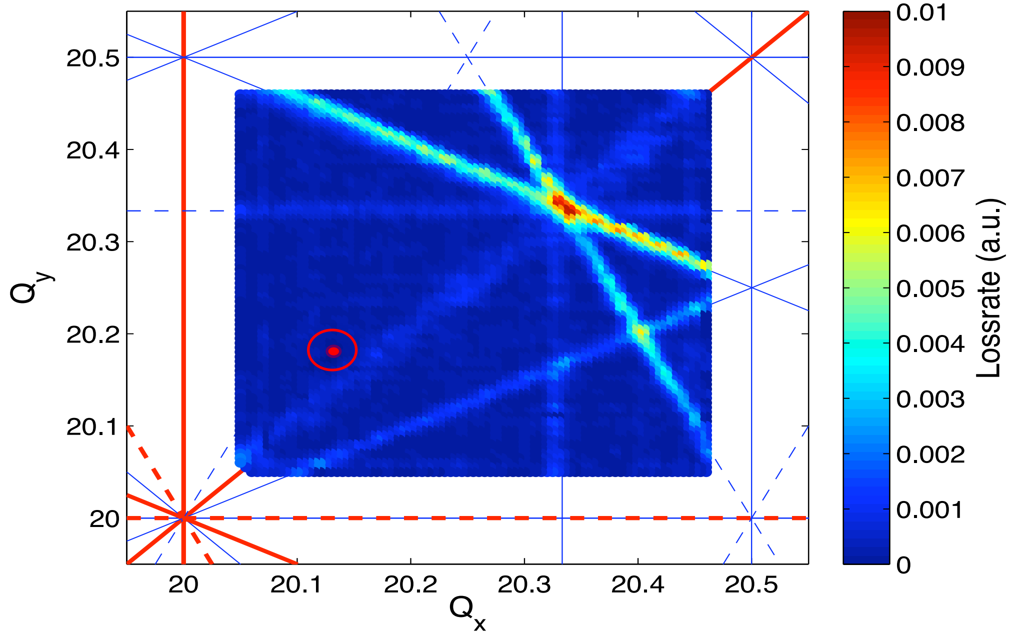

Space charge frequency scan

- Injecting high bunch density beam into the SPS
- Space charge effect quite strong with (linear) tune-shifts of
- Changing horizontal/vertical frequency and measuring emittance (action) blow-up

$\Delta Q_x/\Delta Q_y$ ~ 0.10/0.18

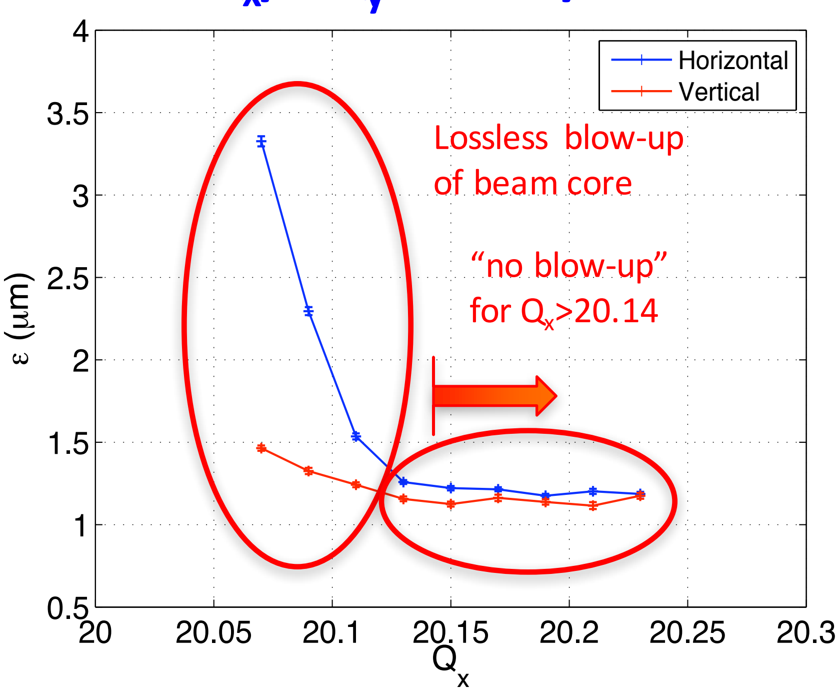

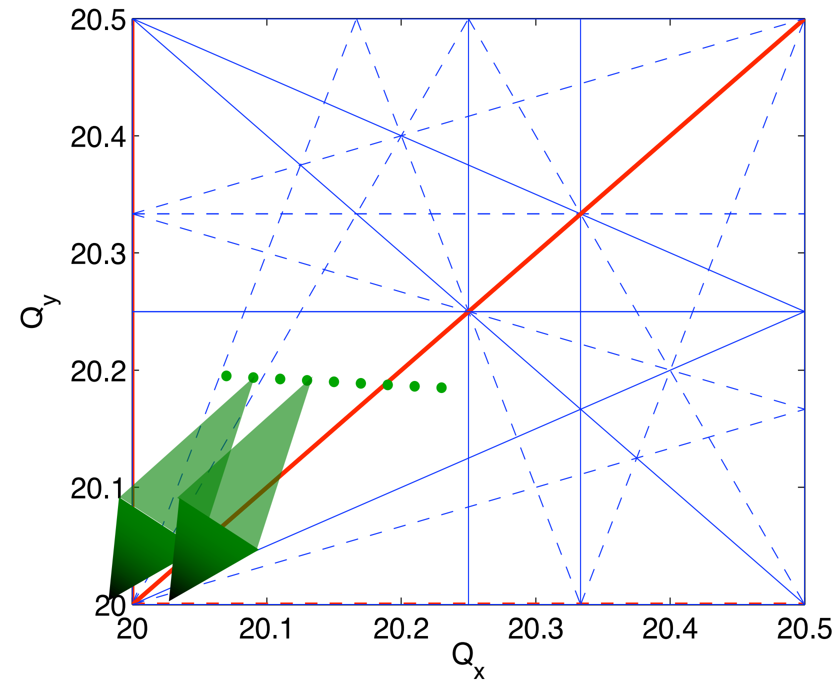

Space charge frequency scan

- Injecting high bunch density beam into the SPS
- Space charge effect quite strong with (linear) tune-shifts of
- Changing horizontal/vertical frequency and measuring emittance (action) blow-up

$\Delta Q_x/\Delta Q_y \sim 0.10/0.18$

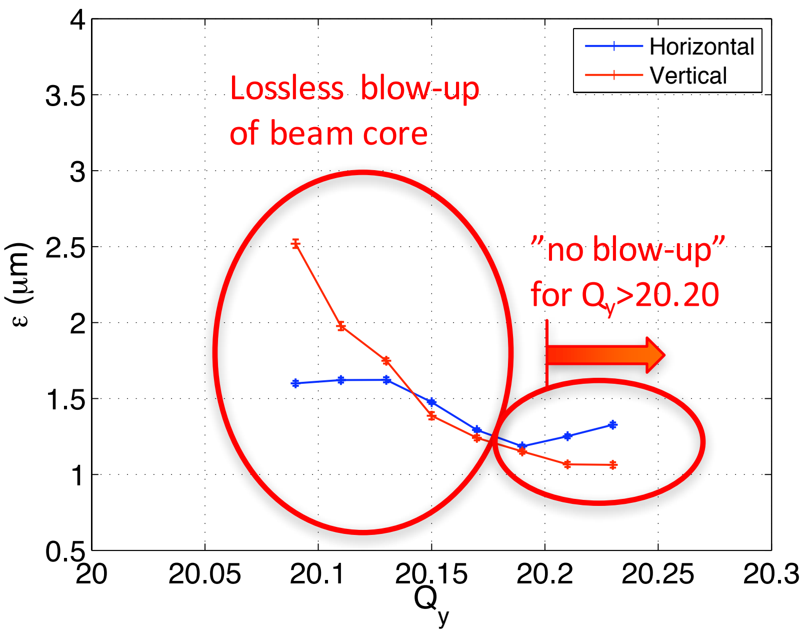

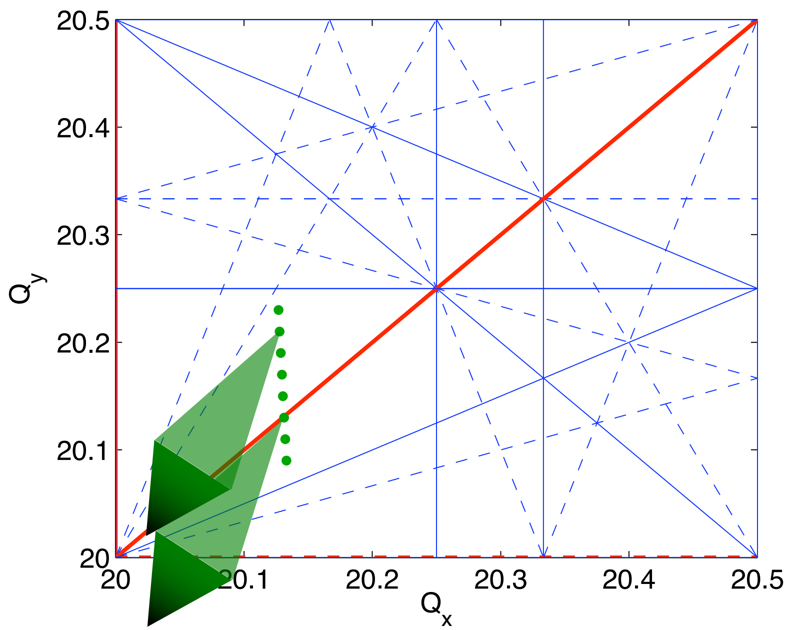

Contents of the 4^{th} lecture

- Chaos detection methods and frequency map analysis
  - Quasi-periodic motion
  - The NAFF algorithm
  - Frequency determination and precision
  - Aspects of frequency maps
- Simulation studies
  - Frequency and diffusion maps for the LHC
  - Beam-beam effect
  - Folded frequency maps
  - Magnet fringe-fields
  - Working point choice
  - Resonance free lattice
  - Symplectic integration
  - Correction schemes evaluation
- Experiments
  - Experimental frequency maps
  - Beam loss frequency maps
  - Space-charge frequency scan
- Summary

Summary

- Frequency map analysis is a powerful technique for analyzing particle motion in simulations but also in real accelerator experiments
- Based on ability to reconstruct numerical quasi-periodic solutions in phase space of general Hamiltonian system
- The power of NAFF algorithm ensures the accurate determination of fundamental frequencies of motions with very high precision precision
- A wide of range of applications for understanding limitations due to non-linear effects in a variety of accelerators
- Application of the method in turn-by-turn data recorded in beam position monitors can reveal effect of non-linear resonances experimentally

Acknowledgments

Thanks for the material to
F.Antoniou, H.Bartosik, W.Herr,
J.Laskar, S.Liuzzo, L.Nadolski,
D.Robin, C.Skokos, C.Steier,
F.Schmidt, A.Wolski,
F.Zimmermann